© 2022. Published by The Company of Biologists Ltd | Development (2022) 149, dev200937. doi:10.1242/dev.200937

RESEARCH ARTICLE

Gata2, Nkx2-2 and Skor2 form a transcription factor network regulating development of a midbrain GABAergic neuron subtype with characteristics of REM-sleep regulatory neurons

Anna Kirjavainen[1,*], Parul Singh[1,*], Laura Lahti[1,*,‡], Patricia Seja[1], Zoltan Lelkes[2,3], Aki Makkonen[4], Sami Kilpinen[1], Yuichi Ono[5], Marjo Salminen[6], Teemu Aitta-Aho[4], Tarja Stenberg[2], Svetlana Molchanova[1], Kaia Achim[1,§] and Juha Partanen[1,§]

ABSTRACT

The midbrain reticular formation (MRF) is a mosaic of diverse GABAergic and glutamatergic neurons that have been associated with a variety of functions, including sleep regulation. However, the molecular characteristics and development of MRF neurons are poorly understood. As the transcription factor, Gata2 is required for the development of all GABAergic neurons derived from the embryonic mouse midbrain, we hypothesized that the genes expressed downstream of Gata2 could contribute to the diversification of GABAergic neuron subtypes in this brain region. Here, we show that Gata2 is required for the expression of several GABAergic lineage-specific transcription factors, including Nkx2-2 and Skor2, which are co-expressed in a restricted group of post-mitotic GABAergic precursors in the MRF. Both Gata2 and Nkx2-2 function is required for *Skor2* expression in GABAergic precursors. In the adult mouse and rat midbrain, *Nkx2-2*-and *Skor2*-expressing GABAergic neurons locate at the boundary of the ventrolateral periaqueductal gray and the MRF, an area containing REM-off neurons regulating REM sleep. In addition to the characteristic localization, *Skor2*$^{+}$ cells increase their activity upon REM-sleep inhibition, send projections to the dorsolateral pons, a region associated with sleep control, and are responsive to orexins, consistent with the known properties of midbrain REM-off neurons.

KEY WORDS: Midbrain reticular formation, Deep mesencephalic nucleus, Periaqueductal gray, Neurogenesis, Transcription factor, Skor2, Nkx2-2, Gata2, REM sleep, Mouse, Rat

INTRODUCTION

Gamma-aminobutyric acid (GABA) is the main inhibitory neurotransmitter in the mature brain and neurons using GABA as their principal transmitter (GABAergic neurons) are widely distributed throughout the central nervous system. In the midbrain, abundant GABAergic neurons are located in the midbrain reticular formation (MRF; also known as the deep mesencephalic nucleus) and the periaqueductal gray (PAG). Very little is known about the subtype-specific features of the GABAergic neurons in the MRF and PAG. This is a major obstacle for understanding the MRF- and PAG-associated brain functions, including regulation of defensive behavior, nociception and sleep (Keay and Bandler, 2001; Luppi et al., 2017). A region at the boundary of the dorsomedial MRF (dMRF) and ventrolateral PAG (vlPAG) contains GABAergic neurons implicated in the regulation of rapid eye movement (REM) sleep. The GABAergic neurons in the dMRF/vlPAG are activated by REM-sleep deprivation, project to other brainstem regions regulating REM sleep and appear to modulate the sleep pattern (Luppi et al., 2017; Saper et al., 2010; Scammell et al., 2017; Weber and Dan, 2016). However, despite their functional importance, limited information is available on the development and differentiation of the MRF and PAG GABAergic neurons, and the subtype-specific molecular features of these cells.

The embryonic midbrain can be divided into dorsoventral progenitor domains differing in their gene expression (m1-m7) (Kala et al., 2009; Nakatani et al., 2007). Of these, the domains m1-m3, ventral m4 and m5 give rise to post-mitotic GABAergic neuron precursors. The development of these GABAergic neuron precursors depends on the function of the zinc-finger transcription factor (TF) Gata2. The expression of Gata2 is activated in midbrain precursors immediately upon their cell cycle exit, and Gata2 drives the GABAergic differentiation over alternative glutamatergic fates (Kala et al., 2009). Gata2 appears to function together with the Tal-family TFs, in particular Tal2, to direct GABAergic neurogenesis in the midbrain (Achim et al., 2013). Although Gata2 and Tal2 are required for the differentiation of all the midbrain GABAergic precursors, the contribution of the precursor subtypes to different brain nuclei, and the gene regulatory circuits guiding the subtype diversification, are unknown.

Here, we identify Gata2-dependent TFs marking midbrain GABAergic precursors and their subtypes. Of these, we focus on a restricted subtype of midbrain GABAergic neurons defined by the co-expression of the homeodomain TF Nkx2-2 and the SKI family TF Skor2 (also known as Corl2 and Fussel18). We show that, in these cells, both Gata2 and Nkx2-2 are required for the expression of *Skor2*. We demonstrate that the Skor2 and Nkx2-2 co-expressing neurons have several characteristics, such as anatomical location at the boundary of dMRF and vlPAG, activation by REM-sleep deprivation, projection to pontine areas controlling REM sleep, and responsiveness to orexin (hypocretin, Hcrt), suggesting that this group of midbrain GABAergic neurons is involved in sleep regulation.

[1]Molecular and Integrative Biosciences Research Programme, Faculty of Biological and Environmental Sciences, PO Box 56, FIN00014-University of Helsinki, Helsinki, Finland. [2]Department of Physiology, PO Box 63, FIN00014-University of Helsinki, Helsinki, Finland. [3]Department of Physiology, Faculty of Medicine, University of Szeged, Szeged, Hungary. [4]Department of Pharmacology, PO Box 63, FIN00014-University of Helsinki, Helsinki, Finland. [5]Department of Developmental Neurobiology, Integrated Cell Biology, KAN Research Institute, 6-8-2 Minatojima-Minamimachi, Chuo-ku, Kobe, Hyogo 650-0047, Japan. [6]Department of Veterinary Biosciences, PO Box 66, FIN00014-University of Helsinki, Helsinki, Finland.
‡Present address: Department of Cell and Molecular Biology, Karolinska Institutet, SE-17177 Stockholm, Sweden.
*These authors contributed equally to this work

§Authors for correspondence (kaia.achim@helsinki.fi; juha.m.partanen@helsinki.fi)

A.K., 0000-0001-7036-2312; L.L., 0000-0003-2929-1975; K.A., 0000-0003-3723-4065; J.P., 0000-0001-8850-4825

Handling Editor: Steve Wilson
Received 11 May 2022; Accepted 15 June 2022

Development (2022) 149, dev200937. doi:10.1242/dev.200937

RESULTS

Gene expression changes in the embryonic midbrain lacking Gata2 function

Gata2 operates high in the gene regulatory network, guiding post-mitotic differentiation of GABAergic neuron precursors in the embryonic midbrain (Kala et al., 2009). To reveal the genes downstream of Gata2, we compared the gene expression in E12.5 control (Ctrl) and *En1*$^{Cre/+}$; *Gata2*$^{flox/flox}$ (*Gata2*^{cko}) mutant mouse midbrain (Fig. 1A,B). Using cDNA microarrays, we found 52 genes downregulated in the *Gata2*^{cko} embryos, either in the ventral midbrain, dorsal midbrain or both (logFC>1.5, adjusted *P*-value<0.05, Table S1; all up- and downregulated genes are listed in Table S2). We performed qRT-PCR analyses of the expression of selected GABAergic neuron markers (*Gata2*, *Gad1*, *Slc32a1*), GATA-associated transcription factors (*Tal1*, *Zfpm1*, *Zfpm2*) and novel genes (*Ptchd4*), across different magnitudes of fold changes. Overall, the fold change of each gene expression between the Ctrl and *Gata2*^{cko} observed in the qRT-PCR correlated well with the fold changes observed in the cDNA microarray comparisons (Fig. S1). The small fold-change of *Gata2* gene expression in the microarray (Fig. S1) is likely due to the fact that the microarray probe detects a truncated non-functional *Gata2* transcript. The qRT-PCR and *in situ* hybridization (ISH) indicated robust downregulation of *Gata2* expression (Fig. S1; Fig. 1G,G′). We further validated the downregulation of selected genes by mRNA ISH (Fig. 1C-O′; Table S1).

TF-encoding genes were abundant among the ones downregulated in the *Gata2*^{cko} mutants (Table S1; 14 out of 52 downregulated genes encode TFs). The gene ontology (GO) term enrichment analysis listed 'sequence-specific DNA binding' (*P*=1.06E-5), 'positive regulation of transcription' (*P*=4.63E-4), 'E-box binding' (*P*=0.009), 'nervous system development' (*P*=0.003) and 'neuron differentiation' (*P*=0.014) among top GO terms (Table S3). As expected, the expression of several genes associated with GABAergic neuron functions (such as *Gad1*, *Gad2*, *Slc32a1*) were downregulated in the *Gata2*^{cko} mutants (Fig. 1D,D′; Table S1).

Gata-associated TFs are broadly expressed in the midbrain GABAergic neuron precursors

To dissect the gene regulatory networks downstream of Gata2, we focused on the downregulated TF genes (Fig. 1B). From those, *Gata3*, *Tal1*, *Tal2*, *Zfpm1* and *Zfpm2* have previously been associated with the function of Gata2 or other Gata factors in different developmental contexts (Chlon and Crispino, 2012; Lahti et al., 2016; Morello et al., 2020; Tikker et al., 2020). ISH analysis showed that these putative Gata2 cofactors were broadly expressed in the embryonic day (E) 12.5 midbrain GABAergic neuron precursors (Fig. 1E,E′,H,H′,J-K′,N,N′). Consistent with the microarray profiling, and our earlier studies in the developing midbrain and diencephalon (Achim et al., 2013; Virolainen et al., 2012), *Tal1* expression was completely abolished in the *Gata2*^{cko} (Fig. 1E,E′). In contrast, *Tal2* expression was only modestly downregulated in the dorsal midbrain sample and was still robustly expressed in the midbrain GABAergic precursors in the *Gata2*^{cko} embryos (Fig. 1H,H′; Table S1), supporting the hypothesis of independent activation of *Gata2* and *Tal2* expression and their position at the top of the gene regulatory hierarchy driving midbrain GABAergic neuron differentiation (Achim et al., 2013).

Both *Zfpm1* and *Zfpm2* encode for zinc-finger proteins associating with the Gata TF complex in other cell types (Chlon and Crispino, 2012). *Zfpm1* and *Zfpm2* transcripts were broadly

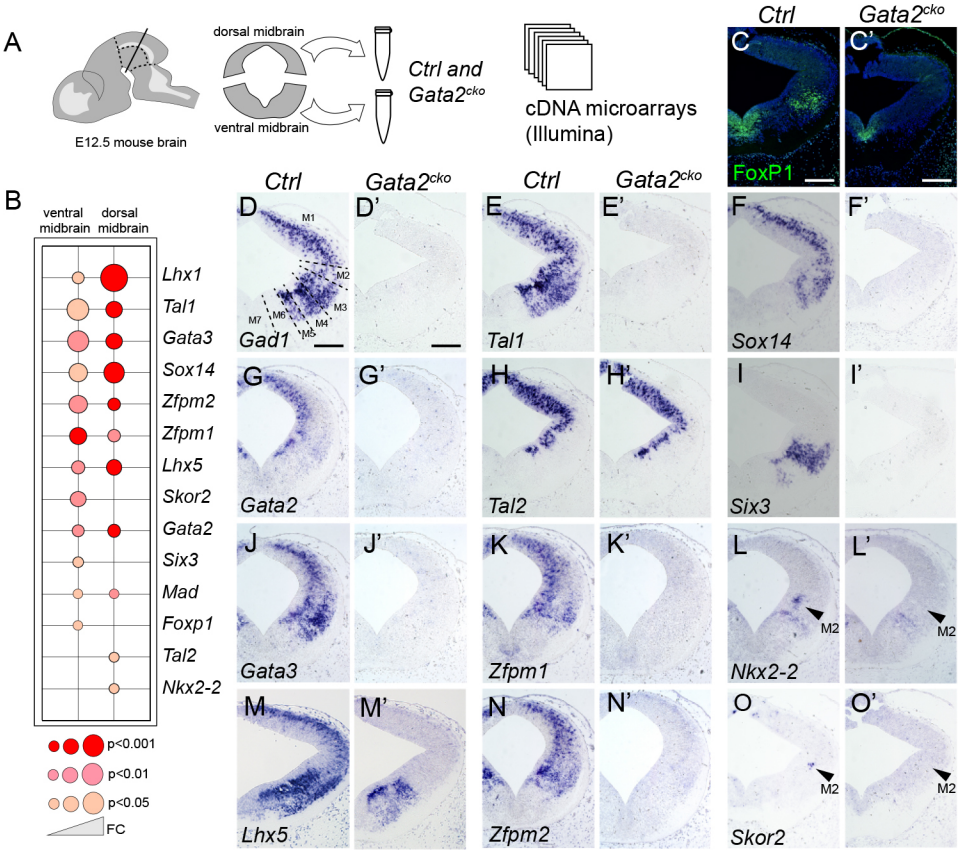

Fig. 1. Gata2-regulated transcription factors in the developing mouse midbrain. (A) Microarray sample collection and experimental design. The dorsal and ventral midbrain tissue from E12.5 Ctrl and *Gata2*^{cko} embryos was collected and analyzed on cDNA microarrays. The samples were collected in three replicates/group, each group consisting of six tissue samples. (B) Downregulated transcription factor genes in the *Gata2*^{cko} midbrain. Gene expression in Ctrl and *Gata2*^{cko} embryos was compared separately in the ventral midbrain and dorsal midbrain samples. Dot size indicates fold change (FC), the color indicates *P*-values. (C-O′) IHC (C,C′) and ISH (D-O′) analysis of the expression of transcription factors identified as downregulated in the *Gata2*^{cko} samples. Analyses were performed on coronal sections of E12.5 Ctrl (C-O) and *Gata2*^{cko} (C′-O′) embryos. Arrowheads on L, L′,O,O′ point to the location of a lateral m2 cell population expressing *Nkx2-2* and *Skor2*, respectively. Scale bars: 100 µm.

Development (2022) 149, dev200937. doi:10.1242/dev.200937

expressed in the GABAergic neuron precursors in E12.5 Ctrl midbrain, but were undetectable in the *Gata2*^{cko} midbrain (Fig. 1K,K′,N,N′). Thus, in the midbrain GABAergic precursors, the expression of several genes encoding for Gata-associated TFs requires Gata2.

Other Gata2-dependent TF genes expressed broadly in the midbrain GABAergic neuron precursors included the LIM-homeobox genes *Lhx1* and *Lhx5* (Fig. 1M,M′). In contrast to *Tal1/2* and *Zfpm1/2*, both *Lhx1* and *Lhx5* were also expressed in the glutamatergic neuron precursors in the m6 and m4 regions, where their expression was not affected by the loss of *Gata2* (Fig. 1M,M′ and Fig. S2).

TFs downstream of Gata2 mark subtypes of mantle zone precursors in the embryonic midbrain

In contrast to the TFs expressed across all midbrain GABAergic neuron precursors, some Gata2-dependent TF genes had more restricted expression patterns. These included *Foxp1*, *Six3*, *Sox14*, *Nkx2-2* and *Skor2*. Using ISH and immunohistochemistry (IHC) analyses at E12.5, we found *Sox14*-expressing precursors primarily in the dorsal midbrain, in particular m1-m3 (Fig. 1F), consistent with earlier studies (Makrides et al., 2018). In turn, we detected precursors expressing *Six3* in the ventrolateral GABAergic domains m3 and m5, *Foxp1* in the m3 and *Nkx2-2* in the m4 and m2 (Fig. 1I,C,L). Notably, *Skor2* showed the most restricted pattern of expression that partially resembled *Nkx2-2* expression in the m2 mantle zone (Fig. 1O). The expression of these TFs was lost in the mantle zone precursors in *Gata2*^{cko} embryos (Figs 1C,C′,F,F′,I,I′,L,L′,O,O′, 2C,F), except for *Nkx2-2*, which was abolished in the m2, but continued in glutamatergic precursors in the m4 domain, as well as proliferative progenitors in the ventral midbrain (Kala et al., 2009).

Varied, combinatorial expression pattern of the Gata2 target genes suggests that the development of diverse populations of midbrain GABAergic neurons entails unique Gata2-dependent TF networks in different post-mitotic GABAergic precursor populations.

Co-expression of *Skor2* and *Nkx2-2* characterizes a specific population of midbrain GABAergic neuron precursors

We next characterized the *Skor2*- and *Nkx2-2*-expressing precursors in more detail. ISH analysis at E12.5 revealed that *Skor2* was expressed in a region coinciding with abundant GABAergic neuron precursors (Fig. 2A,B) and the *Skor2*$^{+}$ post-mitotic precursors in the m2 co-expressed *Gad1* (Fig. 2D), thus representing a subgroup of GABAergic neurons. Combined ISH and IHC analyses indicated that the *Skor2*$^{+}$ post-mitotic neuronal precursors in the m2 co-expressed Nkx2-2 at E12.5 (Fig. 2E). A highly specific subgroup of *Skor2*$^{+}$ *Nkx2-2*$^{+}$ midbrain neurons was detected at E18.5 (Fig. 2G,H,J-M). The *Skor2*, *Nkx2-2* and *Gad1* co-expressing cell population was also found in the adult midbrain (Fig. 2N-O). Similar to E12.5, *Skor2* expression was not detected in the *Gata2*^{cko} midbrain at E18.5 (Fig. 2B,C,H,I), arguing for a fate change and against a delayed differentiation of these neurons in the absence of *Gata2* function. In conclusion, the co-expression of *Skor2* and *Nkx2-2* marks a highly restricted subgroup of Gata2-dependent midbrain GABAergic neurons.

To study the kinetics of differentiation of the *Skor2*$^{+}$ *Nkx2-2*$^{+}$ GABAergic neuron population, we determined the timing of terminal mitosis of the progenitors of these cells. For this, thymidine analogs EdU and BrdU were given at two consecutive days, between E9.5 and E12.5, and their incorporation was analyzed at E13.5. Thymidine analog injection at E9.5-E11.5 efficiently labeled the *Skor2*$^{+}$ *Nkx2-2*$^{+}$ cells, whereas injection at E12.5 labeled only few scattered cells in the posterior midbrain (Fig. S3). These data suggest that *Skor2*$^{+}$ *Nkx2-2*$^{+}$ GABAergic neurons are mostly born between E11.5 and E12.5 and that their cell cycle exit may proceed in an anterior-to-posterior sequence. The birth-dating results are consistent with our gene expression studies that first detected both *Skor2* and *Nkx2-2* expression in the m2 region at ∼E12.0, soon after the terminal mitosis occurs. These results also suggest that the *Skor2*$^{+}$ *Nkx2-2*$^{+}$ GABAergic precursors do not undergo extensive tangential migration, but likely differentiate from the adjacent neuroepithelial progenitors.

Nkx2-2 is required upstream of *Skor2* for the subtype specification of midbrain GABAergic neurons

Next, we asked whether *Nkx2-2* and *Skor2* are required for the differentiation of midbrain GABAergic neurons. We first analyzed *Nkx2-2* null mutant mouse embryos homozygous for an *Nkx2-2*^{Cre} allele (*Nkx2-2*$^{Cre/Cre}$) combined with an *Ai14*^{TdTomato} reporter allele, which expressed red fluorescence protein (RFP) upon Cre-mediated recombination and allowed us to follow the development of the mutant cells. At E12.5, we detected an RFP-labeled cell cluster in the m2 domain, both in the Ctrl (*Nkx2-2*$^{Cre/+}$; *Ai14*$^{TdTomato/+}$) and *Nkx2-2*^{null} (*Nkx2-2*$^{Cre/Cre}$; *Ai14*$^{TdTomato/+}$) embryos (Fig. 3A-C, A′-C′). Although in the Ctrl midbrain the labeled precursors expressed *Skor2*, we could not detect *Skor2* expression in the labeled precursors in the *Nkx2-2*^{null} midbrain (Fig. 3D,D′). Similar to E12.5, *Skor2*-expressing cells were not detected in the midbrain of *Nkx2-2*^{null} embryos at E18.5 (Fig. 3I-J; Fig. S4). This argues against delayed activation of *Skor2* in the *Nkx2-2*-deficient precursors, and suggests that Nkx2-2 is functionally required for *Skor2* transcription in the m2.

To study the neurotransmitter identity of the m2 precursors in the absence of Nkx2-2, we analyzed the midbrain of E12.5 *Nkx2-2*^{null} embryos for the expression of the GABAergic neuron marker *Gad1* and glutamatergic neuron marker *Vglut2* (*Slc17a6*). The m2 precursors labeled by *Nkx2-2*^{Cre} expressed *Gad1*, but not *Vglut2*, both in the Ctrl and the *Nkx2-2*^{null} embryos (Fig. 3E-H,E′-H′). Thus, in the absence of Nkx2-2 function, the m2 precursors still acquire a GABAergic identity. However, the GABAergic subtype identity of m2 derivatives appears to be altered as the *Skor2* expression is lost.

To study whether Skor2 is required for the *Nkx2-2* expression and differentiation of the m2 precursors, we used mice carrying a *Skor2*^{GFP} allele (Nakatani et al., 2014), in which the coding sequences of *Skor2* are replaced with enhanced green fluorescent protein (EGFP). Neither *Skor2* mRNA nor Skor2 protein was detected in *Skor2*$^{GFP/GFP}$ embryos, confirming the loss of Skor2 function. At E12.5, EGFP^{+} cells expressing Nkx2-2 and *Gad1* were found in the m2 domain in both *Skor2*$^{GFP/+}$ and *Skor2*$^{GFP/GFP}$ embryos (Fig. 3K-P,K′-P′) and the number of cells expressing GFP and Nkx2-2 did not differ between the *Skor2*$^{GFP/+}$ and *Skor2*$^{GFP/GFP}$ embryos at E12.5 (Fig. 3Q). We did not observe major differences in the appearance of GFP-expressing cell clusters or cell morphology between the *Skor2*$^{GFP/+}$ and *Skor2*$^{GFP/GFP}$ embryos at E18.5 (Fig. S5). Thus, the prospective *Skor2, Nkx2-2*-expressing cell lineage was maintained in the absence of *Skor2* function. Furthermore, analyses of *Vglut2* and *Gad1* expression indicated that the E18.5 *Skor2*$^{GFP/GFP}$ cells retained their GABAergic identity (Fig. 3R-S′, filled arrowheads).

Development (2022) 149, dev200937. doi:10.1242/dev.200937

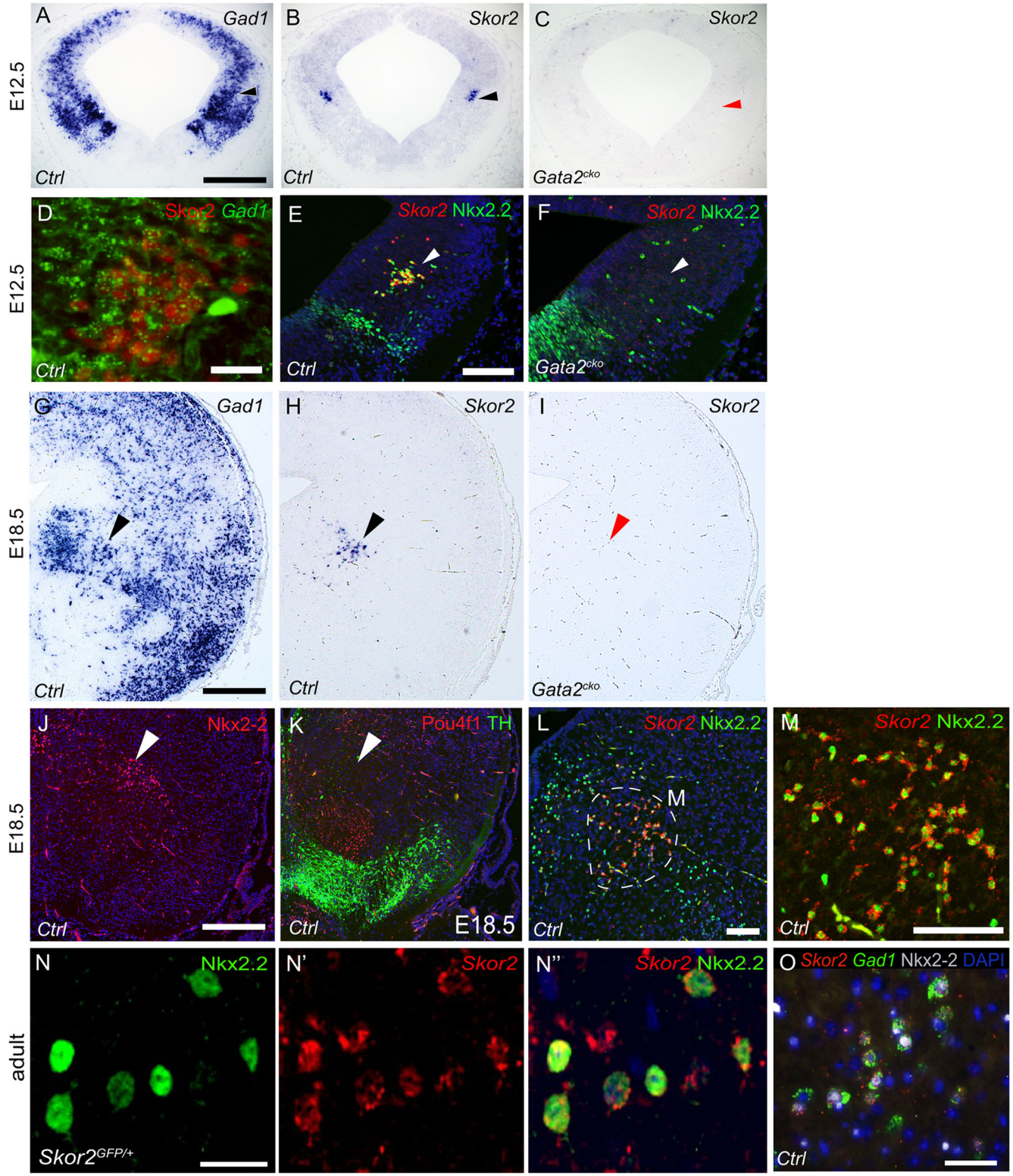

Fig. 2. *Skor2* and *Nkx2-2* are co-expressed in a Gata2-dependent fashion in a subtype of lateral midbrain GABAergic precursors. (A,B) Expression of *Gad1* (A) and *Skor2* (B) analyzed by ISH on parallel coronal sections of an E12.5 Ctrl embryo. (C) Loss of *Skor2* expression in an E12.5 *Gata2*^{cko} embryo. (D) Co-expression of Skor2 (IHC) and *Gad1* (ISH). Skor2 is detected in a subset of *Gad1*-expressing cells in the lateral midbrain. (E,F) Co-expression of Nkx2-2 (IHC) and *Skor2* (ISH) on E12.5 Ctrl and *Gata2*^{cko} midbrain. The expression of both genes is lost in the *Gata2*^{cko} lateral midbrain m2 domain (arrowhead). (G) *Gad1* expression (ISH) on a coronal section of E18.5 Ctrl midbrain. (H,I) *Skor2* expression (ISH) on a coronal section of E18.5 Ctrl and *Gata2*^{cko} midbrain. (J,K) Nkx2-2 (IHC) and tyrosine hydroxylase (TH) and Pou4f1 (co-IHC) expression on adjacent coronal sections of E18.5 Ctrl embryo. The arrowheads point to the expected position of the *Skor2*$^{+}$ cell population. (L,M) Co-expression of *Skor2* (ISH) and Nkx2-2 (IHC) in the E18.5 mouse midbrain. M shows a close-up of the double labeled cells circled in L. (N-N″) Co-expression of Nkx2-2 (IHC) and *Skor2* (ISH) in the dMRF/vlPAG of adult mouse midbrain, in a region corresponding to the position of *Skor2*$^{+}$ cells in the E18.5 brain. (O) Co-expression of Nkx2-2 (IHC), *Skor2* (ISH) and *Gad1* (ISH) in the dMRF/vlPAG of adult mouse midbrain. Scale bars: 200 µm (A-C,G-K); 50 µm (D-F,L,M,O); 20 µm (N-N″).

Development (2022) 149, dev200937. doi:10.1242/dev.200937

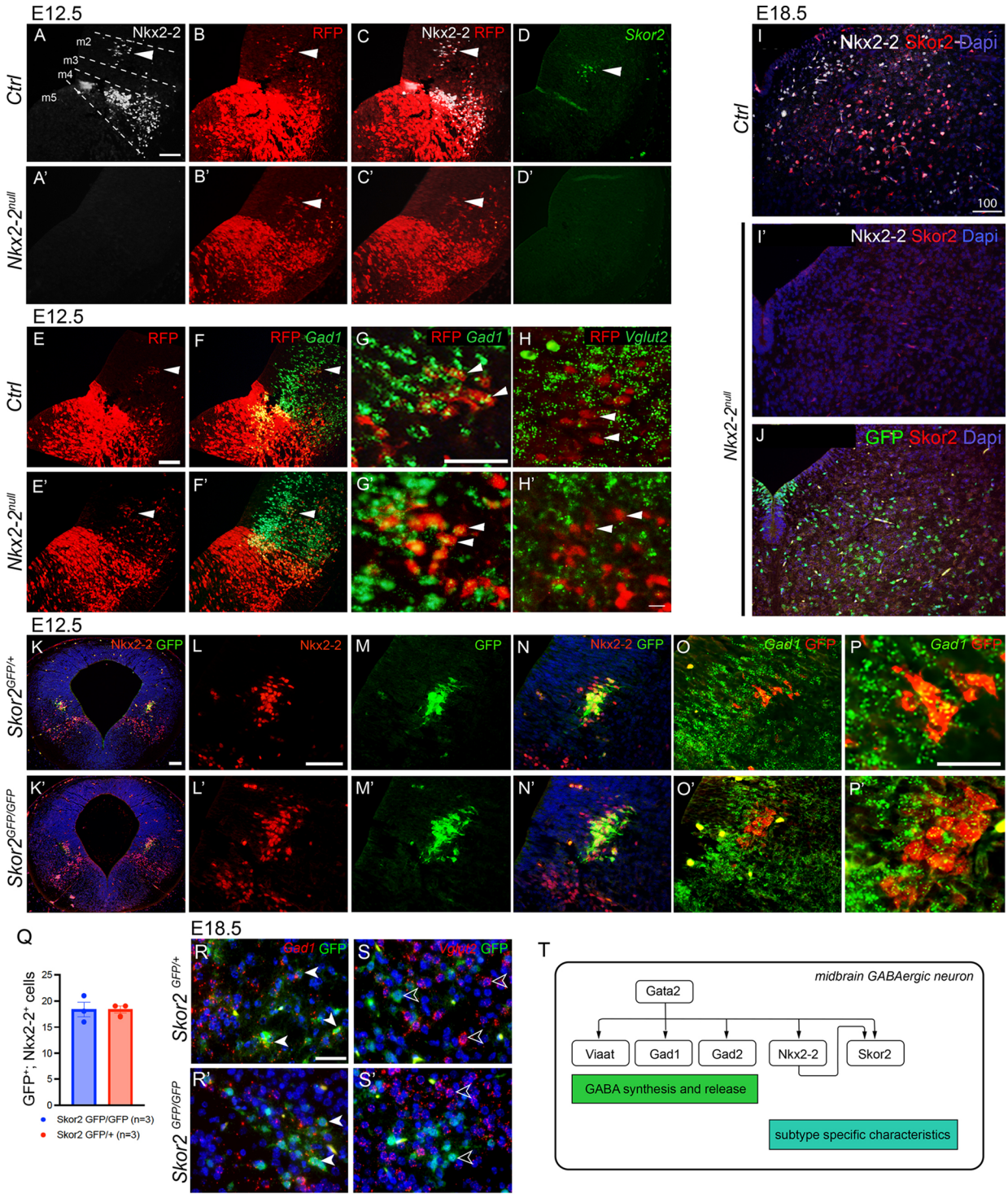

Fig. 3. The function of *Nkx2-2* and *Skor2* in the developing midbrain GABAergic precursors. (A-D′) Nkx2-2 is required for *Skor2* expression in the m2. IHC for Nkx2-2 and RFP in the E12.5 Ctrl (*Nkx2-2*$^{Cre/+}$, *Ai14*$^{TdTomato\ /+}$) and *Nkx2-2*^{null} (*Nkx2-2*$^{Cre/Cre}$, *Ai14*$^{TdTomato\ /+}$) midbrain (A-C′) indicates that Nkx2-2 lineage precursors, marked by RFP expression, are generated in the midbrain m2 domain of the *Nkx2-2*^{null} embryos, but they lack *Skor2* expression (ISH) (arrowheads). (E-H′) Expression of *Gad1* (F-G′) and *Vglut2* (H,H′) in the *Nkx2-2* lineage cells is unaltered by the loss of Nkx2-2 function. ISH for *Gad1* or *Vglut2* combined with IHC for RFP in the Ctrl and *Nkx2-2*^{null} midbrain at E12.5. (I,I′) Expression analysis of Skor2 (IHC) and Nkx2-2 (IHC) in E18.5 Ctrl and *Nkx2-2*^{null} midbrain. Skor2 expression is lost in the *Nkx2-2*^{null} midbrain. (J) Expression analysis of Skor2 (IHC) and *Nkx2-2* (IHC for GFP transcribed from the *Nkx2-2*^{Cre} allele, where both Cre and EGFP sequences are inserted into the *Nkx2-2* locus) in E18.5 *Nkx2-2*$^{Cre/Cre}$ midbrain. (K-N′) Co-expression of Nkx2-2 (IHC) and *Skor2* (IHC for GFP encoded by the *Skor2*^{GFP} allele) in E12.5 *Skor2*$^{GFP/+}$ (Ctrl) and *Skor2*$^{GFP/GFP}$ midbrain. (O-P′) Co-expression of *Gad1* (ISH) and *Skor2* (IHC for GFP encoded by the *Skor2*^{GFP} allele) in E12.5 *Skor2*$^{GFP/+}$ and *Skor2*$^{GFP/GFP}$ midbrain. (Q) Number of cells co-expressing GFP and Nkx2-2 in the E12.5 *Skor2*$^{GFP/+}$ and *Skor2*$^{GFP/GFP}$ animals. Data are mean±s.d. (R-S′) Analysis of GFP (IHC), *Vglut2* (ISH) and *Gad1* (ISH) expression in the midbrain of E18.5 *Skor2*$^{GFP/GFP}$ and *Skor2*$^{GFP/+}$ (Ctrl) embryos. *Skor2* mutant cells maintain their GABAergic identity. Filled arrowheads point to *Gad1* GFP double labeled cells, empty arrowheads to GFP+ or *Vglut2*+ single labeled cells. (T) A schematic of the transcriptional regulatory network in differentiating midbrain m2 GABAergic neurons. Scale bars: 50 µm (A-H′,L-P′, R-S′); 100 µm (I-J); 200 µm (K,K′).

Development (2022) 149, dev200937. doi:10.1242/dev.200937

Together, these results show that, in the differentiating midbrain m2 precursors, Nkx2-2 is required upstream of Skor2. The cell cycle exit, cell survival and GABAergic neurotransmitter fate specification of the m2 precursors appear to be independent of Nkx2-2 and Skor2. Instead, these TFs might regulate acquisition of GABAergic subtype-specific neuronal characteristics (Fig. 3T).

Skor2-expressing GABAergic neurons are located at the boundary of the dMRF and vlPAG

The expression of *Skor2* and Nkx2-2 in a highly restricted population of embryonic midbrain GABAergic precursors likely signifies the development of an anatomically and functionally distinct subtype of GABAergic neurons. Therefore, we asked whether *Skor2*$^{+}$ *Nkx2-2*$^{+}$ neurons are located in unique midbrain GABAergic nuclei in the postnatal brain.

We detected EGFP expression in the postnatal day (P) 4 and adult *Skor2*$^{GFP/+}$ mice, demonstrating specific *Skor2* expression in a subset of GABAergic neurons in the dMRF and in the adjacent vlPAG region of the midbrain (Fig. 4A-G). *Skor2*$^{+}$ cells were found throughout the midbrain, with their number decreasing caudally (Fig. 4B-D,H). In the mouse midbrain, cells were concentrated at the boundary of the PAG, as indicated by anatomical landmarks including expression of neurofilament and tyrosine hydroxylase (Fig. 4E). *Skor2* was also expressed in the cerebellar Purkinje cells and uncharacterized nuclei in the ventral hindbrain both in the mouse (Fig. 4H) and in the rat (Fig. S6). In addition to the mouse, we analyzed *Skor2* and *Nkx2-2* expression in the rat, and verified that both genes are specific to the embryonic m2 mantle zone and adult dMRF/vlPAG in the E15.5 rat midbrain (Fig. 4I,J).

REM-sleep deprivation activates the *Skor2*-expressing neurons in the dMRF/vlPAG

GABAergic neurons at the boundary of the dMRF and the vlPAG have been implicated in inhibition of REM sleep and control of transitions between REM and non-REM sleep (Boissard et al., 2003; Hayashi et al., 2015; Lu et al., 2006; Weber et al., 2018). The activity of these REM-off neurons is increased by experimental REM-sleep deprivation, as demonstrated by upregulation of c-Fos (Fos) expression (Sapin et al., 2009). As the anatomical location of the REM-off neurons appears to be very similar to the location of *Skor2*$^{+}$ and *Nkx2-2*$^{+}$ neurons at the dMRF/vlPAG boundary, we hypothesized that the *Skor2*$^{+}$ *Nkx2-2*$^{+}$ neurons represent the REM-off neurons. To test this, we asked whether c-Fos expression was affected in the *Skor2*-expressing cells by REM-sleep deprivation. For this, we implemented the REM-sleep deprivation model using the inverted flowerpot method established for the rat (Sapin et al., 2009) (Fig. 4K). We analyzed the co-expression of c-Fos, *Nkx2-2* and *Skor2* in the dMRF/vlPAG in the REM-sleep deprived rats (Fig. 4L,M-R‴). The comparison of the proportion of dMRF/vlPAG *Skor2*$^{+}$ neurons expressing c-Fos revealed a significant increase in c-Fos expression in the REM-sleep deprived rats (n=6, 72 h deprivation of REM sleep) compared with the control groups [dry control (DC) n=5; large platform control (LPC) n=6], and a recovery group [72 h REM-sleep deprivation followed by 9 h period of normal sleep conditions (REMSD+Rec) n=3] (Fig. 4S, Kruskal–Wallis H=12.399, P=0.0061; Fig. S7 and Table S4).

Skor2-expressing neurons in the dMRF/vlPAG project to the dorsolateral pons

Earlier studies have shown that dMRF/vlPAG GABAergic neurons project to the dorsolateral pons and inhibit its REM-sleep promoting activity (Boissard et al., 2003; Hayashi et al., 2015; Lu et al., 2006; Sapin et al., 2009; Weber et al., 2018). To test whether the *Skor2*-expressing GABAergic cells in the dMRF/vlPAG project to the dorsolateral pons, we injected the retrograde tracer Choleratoxin subunit B (CtB) to the dorsolateral pons of adult *Skor2*$^{GFP/+}$ mice (Fig. 5A,B). We then quantified the CtB incorporation rate in the dMRF/vlPAG region. In the injected animals (n=6), CtB label was detected in 38.5%±4.8% (mean±s.d.) of the cells in the dMRF/vlPAG region (Fig. 5C), consistent with the dorsolateral pons receiving inputs from the dMRF. Of the *Skor2*$^{+}$ dMRF/vlPAG neurons, 33.8%±4% incorporated CtB (Fig. 5C-D″, arrowheads), confirming that the *Skor2*$^{+}$ dMRF/vlPAG neurons also project to the dorsolateral pons. However, the *Skor2*$^{+}$ cells are clearly not the only dMRF/vlPAG neuron type projecting to the dorsolateral pons, as of the *Skor2*$^{-}$ dMRF/vlPAG neurons, 40.8%±5.9% incorporated CtB.

Skor2^{+} neurons express functional orexin receptors

Orexinergic signaling via the orexin receptors (Hcrtr1 and Hcrtr2) regulates sleep and wakefulness, and loss of the hypothalamic orexinergic neurons is associated with narcolepsy with cataplexy, possibly because of altered input to vlPAG GABAergic neurons that express orexin receptors (Kaur et al., 2009; Lu et al., 2006). We analyzed the expression of Hcrtr1 and Hcrtr2 in the dMRF/vlPAG of adult *Skor2*$^{GFP/+}$ mice (n=4) using IHC (Fig. 6A-B″). We found that, compared with *Skor2*$^{-}$ cells, a significantly larger proportion of the *Skor2*$^{+}$ cells expressed Hcrtr1 and Hcrtr2. Of the *Skor2*$^{+}$ cells, 68.5%±1.6% expressed Hcrtr1 and 69.5%±0.7% expressed Hcrtr2 (Fig. 6C,D). As the proportion of both *Skor2*$^{+}$/Hcrtr1^{+} and *Skor2*$^{+}$/Hcrtr2^{+} double positive neurons were above 50% in all animals (n=4), the co-expression of both receptors is likely, but not analyzed here. Of the *Skor2*$^{-}$ cells in the dMRF/vlPAG, 23.2% expressed Hcrtr1 and 26.2% expressed Hcrtr2 (Fig. 6C,D).

We next asked whether the *Skor2*$^{+}$ cells respond to orexin. In voltage clamp recordings of acute midbrain slices of adult *Skor2*$^{GFP/+}$ mice, bath application of orexin A (1 µM) induced an inward current in the GFP-expressing *Skor2*$^{+}$ cells, but not the neighboring control cells (−10.9±1.7 pA versus −2.2±0.9 pA, P<0.001; Fig. 6E,F). The proportion of responding cells (Skor2^{+}: 32/44 cells, 72%; Skor2^{-}: 0/14 cells) correlated with the proportion of the *Skor2*$^{+}$ cells expressing orexin receptors.

Functionally and anatomically distinct subtypes of *Skor2*$^{+}$ neurons

Finally, we characterized the firing properties of the *Skor2*$^{+}$ cells (n=42) in the dMRF/vlPAG region in acute midbrain slices of adult *Skor2*$^{GFP/+}$ mice (n=17) using a whole cell patch clamp. We then compared the obtained passive and active membrane properties among the measured cells, and saw some clear differences in patterns of action potential firing. Because of the heterogeneity of the neurons, we decided to divide the cells into three subgroups, referred to here as adapting (n=13), stuttering (n=14) and intermediate neurons (n=15) (Fig. 7A-D). Cells were assigned to the stuttering group, if they displayed fast-decaying afterhyperpolarizing potential (AHP) and exhibited characteristic stuttering action potential firing with bursts of action potentials (APs) intermingled with quiescent periods. The rest of the cells had AHP with longer decay and fired action potentials in adapting mode, with regular AP intervals becoming longer towards the end of the current step. Cells were assigned to the adapting group if their AHP consisted of two clear components, separating fast and medium AHP. The rest of the cells, displaying adapting firing and AHP without two components, were placed to the intermediate

Development (2022) 149, dev200937. doi:10.1242/dev.200937

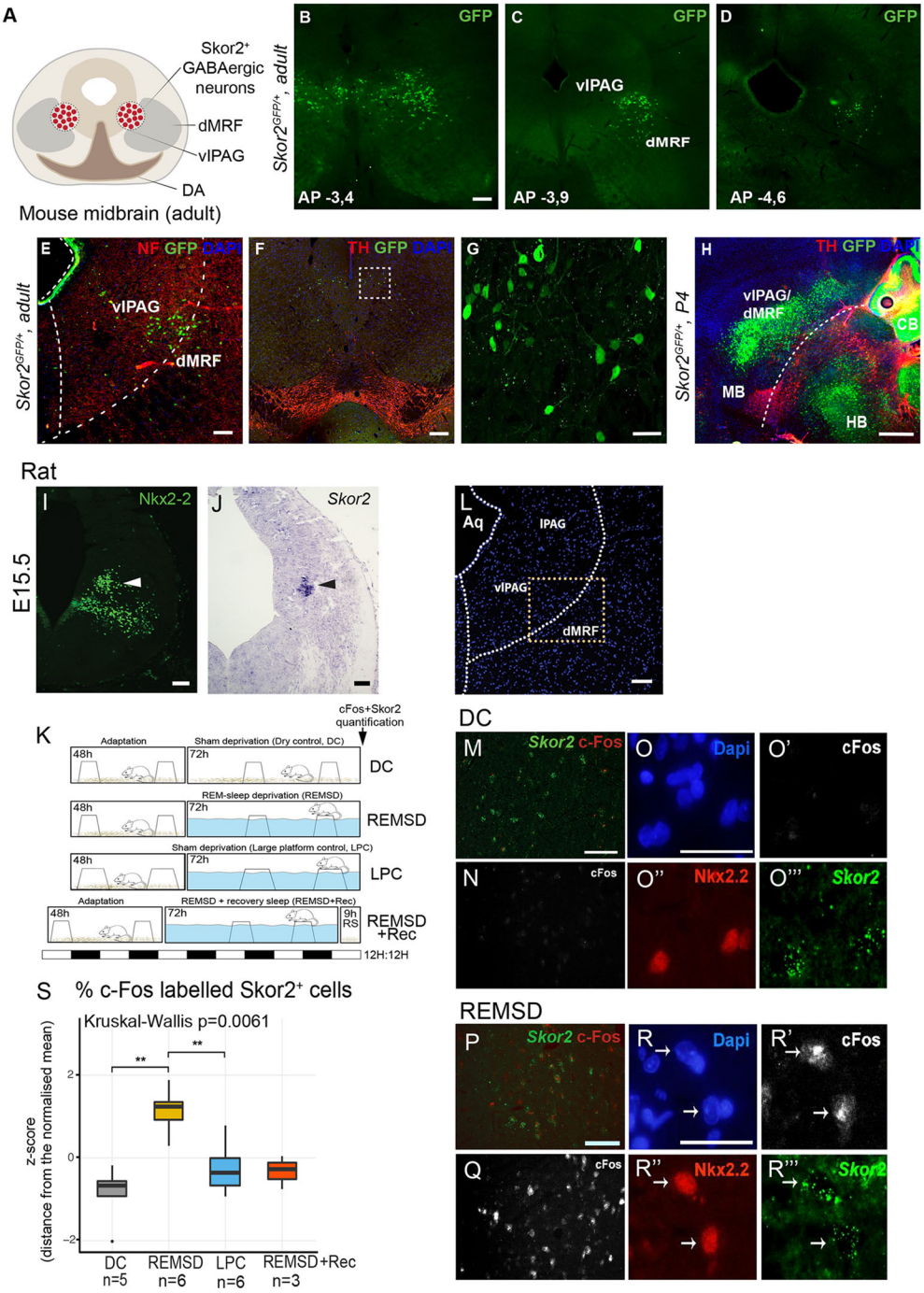

Fig. 4. *Skor2*-expressing neurons are located at the boundary of dMRF and vlPAG in the adult brain and their activity is increased by REM-sleep deprivation. (A) Schematic coronal section of an adult mouse midbrain, indicating the position of the *Skor2*$^{+}$ cells. (B-D) Analysis of GFP expression (IHC) in coronal sections of the adult *Skor2*$^{GFP/+}$ mouse brain. The distance from the bregma is indicated on each section. (E-G) Analysis of GFP expression in relation to neurofilament (NF; E) and tyrosine hydroxylase (TH; F) expression (IHC) in coronal sections of the adult *Skor2*$^{GFP/+}$ mouse midbrain. The vlPAG and dMRF regions are indicated. (G) Close-up of the GFP^{+} cells located in the area indicated in F (dashed square). (H) Sagittal section of the P4 *Skor2*$^{GFP/+}$ mouse brain analyzed for the expression of TH and GFP (IHC). Midbrain (MB), hindbrain (HB) and cerebellum (CB) are indicated. (I,J) Nkx2-2 (IHC) and *Skor2* (ISH) expression on coronal sections of the E15.5 rat midbrain. Arrowheads point to the position of the *Skor2*$^{+}$ cell population. (K) Schematic presentation of the REM-sleep deprivation assay. The experimental groups include the REM-sleep deprived rats (REMSD) housed in a cage with small platforms preventing the animals from entering REM-sleep, two control groups (dry control, DC, and large platform control, LPC) housed in conditions allowing REM-sleep, and a group allowed to have REM-sleep after REM-sleep deprivation (REMSD+Rec). Treatment times are indicated in the boxes. The bar below shows the light-dark cycle in the experiments. (L) Coronal section of adult rat midbrain showing the area analyzed for *Skor2* and c-Fos expression (vlPAG/dMRF). Aq, aqueduct; lPAG, lateral PAG. (M-R‴) Representative images of c-Fos (IHC), Nkx2-2 (IHC) and *Skor2* (ISH) expression in the DC and REMSD rats. All sections are from the dMRF area; low magnification and high magnification is shown per area and experimental group. c-Fos^{+} Skor2^{+} cells were counted from the co-stained sections covering the whole dMRF area to obtain data for the quantifications shown in S. (S) The proportion of *Skor2*$^{+}$ cells that express c-Fos in the REMSD and REMSD+Rec rats and the control groups (DC, LPC). Scale bars: 100 µm (B-D,F); 50 µm (E,G,I,J,L-R‴); 500 µm (H).

Development (2022) 149, dev200937. doi:10.1242/dev.200937

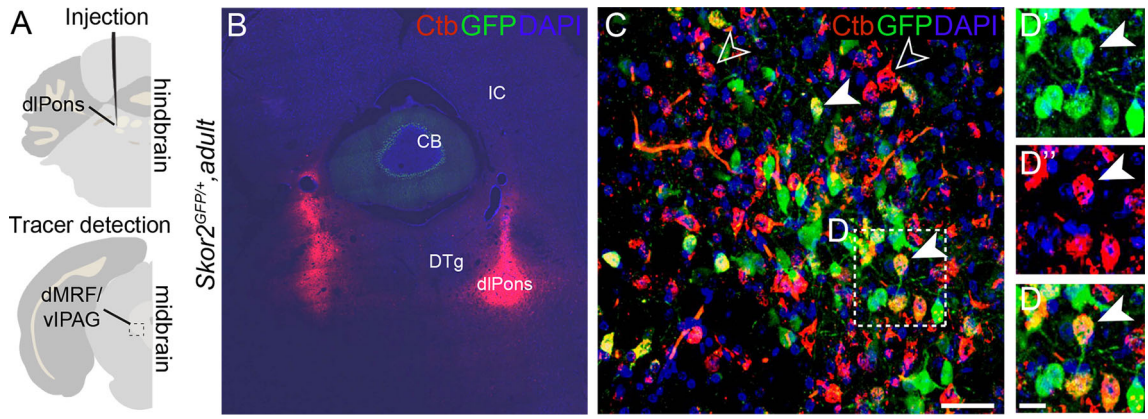

Fig. 5. Retrograde labeling of the dMRF/vlPAG *Skor2*$^{+}$ neurons from the dorsolateral pons. (A) Experiment design for the retrograde labeling. CtB tracer was injected in the dorsolateral pons (dlPons) in the hindbrain of adult *Skor2*$^{GFP/+}$ mice (n=6). dMRF/vlPAG area in the midbrain was analyzed for the tracer expression. (B) Injection site after CtB injection. CB, cerebellum; DTg, dorsal tegmental nucleus; IC, inferior colliculus. (C) dMRF region analyzed for the expression of GFP and CtB (IHC) 5 days after injection. (D-D″) Examples of double labeled cells, from the area indicated in C (dashed square). Individual staining for GFP (D′) and CtB (D″) and the merged image (D) are shown. Filled arrowheads point to the Skor2 CtB double labeled cells, empty arrowheads to the CtB-labeled Skor2-GFP^{-} cells. Scale bars: 10 µm (C,D).

group. The division of cells into three subgroups was supported by a statistically significant difference in individual parameters of AP firing. Adapting neurons had the highest rate of spontaneous activity (adapting: 7.5±1.4 Hz, stuttering: 0.7±0.3 Hz, intermediate: 4.7±1 Hz) and the lowest rheobase (adapting: 31.5±6 pA, stuttering: 92.1±13.7 pA, intermediate: 56.7±7.9 pA) (Fig. 7E-H). The neuron classes also significantly differ in the amplitude of the medium AHP (adapting: 15.1±0.8 mV, stuttering: 7.4±0.7 mV, intermediate 12.3±0.9 mV) and voltage response to hyperpolarizing current steps (slope of the linear I-V relationship, adapting: 0.6±0.1 mV/pA, stuttering: 0.3±0.04 mV/pA, intermediate: 0.4±0.05 mV/pA). Other passive and active membrane properties were similar (Fig. S8). The kinetics of the afterhyperpolarization, as well as hyperpolarization-induced currents, suggest a differential expression of unknown K^{+} channels in the *Skor2*$^{+}$ neuron subgroups.

To morphologically characterize the *Skor2*$^{+}$ cells, we filled the recorded cells with biocytin, allowing visualization of their neurites in the midbrain slices. Sholl analysis of the biocytin-filled cells (n=44, cells from 16 animals) suggested that, as a group, the GFP-expressing *Skor2*$^{+}$ neurons (n=35) did not significantly differ from the neighboring neurons negative for GFP expression (n=9; Fig. S9A-C). However, we detected differences among the *Skor2*$^{+}$ neuron subgroups with different firing patterns. The adapting neurons exhibited a slightly higher number of intersections compared with intermediate or stuttering neurons (Fig. 7I). The most significant differences were observed between adapting and intermediate neurons in a zone 20-120 µm and 170-380 µm from the soma (Kruskal–Wallis, P<0.01; Fig. 7I; Fig. S9D-G). However, no statistically significant differences were detected in the total neurite numbers or total neurite lengths of the three *Skor2*$^{+}$ neuron subgroups (Fig. 7J,K). Considering that the Skor2^{+} cells might be long-range projection neurons, the thickness of the slice (250 µm) likely limits their full morphological characterization here. We also mapped the localization of the *Skor2*$^{+}$ neurons relative to the ventricle. Our results suggest that, compared with the intermediate neurons, the adapting neurons are localized further away from the ventricle (Fig. 7L). Thus, the adapting neurons show the longest projections and appear to localize primarily in the dMRF rather than in vlPAG (Fig. 7M).

In summary, the *Skor2*$^{+}$ cells in the mouse dMRF/vlPAG region are morphologically and physiologically diverse. A large proportion of the *Skor2*$^{+}$ cells are responsive to orexin via Hcrtr1/2 and could thus represent the orexin-responsive neurons regulating sleep.

DISCUSSION

The central regions of the midbrain, the PAG and MRF, contain neurons that are important for regulation of multiple aspects of behavior, including defensive behaviors, motivated behaviors, attention and sleep. However, studies of these neurons are hampered by the lack of knowledge on their subtype-specific molecular features and developmental regulation. Gata2 acts as a selector gene required for the differentiation of all midbrain-derived GABAergic lineages, but the mechanisms of subtype-specific fate regulation in those lineages have not been resolved. Here, we have identified several Gata2-regulated and GABAergic subtype-specific TFs, including Nkx2-2 and Skor2. We show that Gata2, Nkx2-2 and Skor2 mark and regulate the development of an anatomically restricted dMRF/vlPAG GABAergic neuron population potentially involved in regulation of REM sleep.

Gene regulatory hierarchy between Gata2, Nkx2-2 and Skor2

We showed that the differentiation of *Skor2*-expressing GABAergic neurons is dependent on both *Gata2* and *Nkx2-2* gene function. In the ventral midbrain, including the m4 region, *Nkx2-2* is expressed in the ventricular zone progenitors as a part of the homeodomain TF code of patterning the ventral neural tube (Kala et al., 2009; Nakatani et al., 2007; Prakash et al., 2009; Puelles et al., 2004). In post-mitotic precursors derived from the m4, *Nkx2-2* expression is maintained after the cell cycle exit and expressed during the subsequent development of both GABAergic and glutamatergic neurons, which remain to be anatomically and functionally characterized. In contrast, in the m2, *Nkx2-2* and *Skor2* were activated only in the post-mitotic precursors in a Gata2-dependent fashion. With the genetic loss-of-function analyses, we demonstrated that the *Nkx2-2* null mutant embryos lose *Skor2* expression, but *Nkx2-2* expression is retained in the absence of *Skor2* gene function. These results indicate a regulatory cascade in which both *Nkx2-2* and *Skor2* genes are activated after the cell-cycle exit, when Gata2 directly or indirectly activates *Nkx2-2*, which

Development (2022) 149, dev200937. doi:10.1242/dev.200937

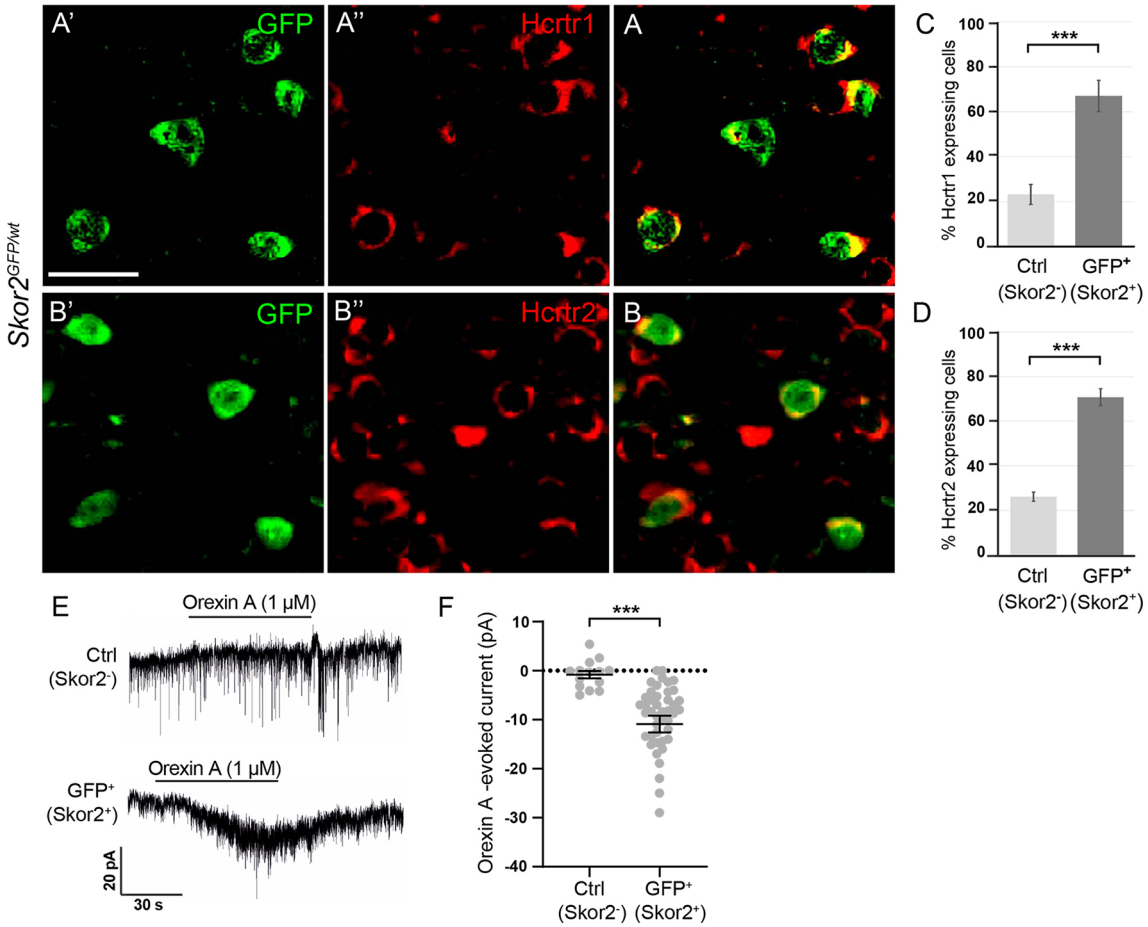

Fig. 6. Orexin receptor expression and orexin-evoked currents in *Skor2*$^{+}$ neurons. (A-B″) Analysis of the co-expression of GFP and Hcrtr1 (A) or Hcrtr2 (B) (IHC) in the dMRF/vlPAG region of the adult *Skor2*$^{GFP/+}$ mice. (C,D) Proportion of Hcrtr1 (C) and Hcrtr2 (D) expressing Skor2^{-} (Ctrl) and Skor2^{+} (GFP+) cells in the dMRF/vlPAG region. Data are mean±s.d. (E) Representative traces of holding currents during orexin A application in GFP^{-} (Ctrl) and GFP^{+} (*Skor2*$^{+}$) cells. (F) Summary of orexin A-induced currents (individual values and mean±s.e.m.) in GFP^{-} (control, *n*=14 cells, three animals) and GFP^{+} (*Skor2*$^{+}$, *n*=44 cells, nine animals) cells. ***P<0.001 (one-way ANOVA on ranks). Scale bar: 50 µm.

in turn regulates the expression of *Skor2*. However, to demonstrate a direct regulatory cascade, chromatin association experiments would be needed to test the binding of Gata2 on the *Nkx2-2* and Nkx2-2 on *Skor2* gene regulatory elements. Furthermore, target genes of Skor2 TF in the vlPAG/dMRF lineage are currently unknown.

The generic GABAergic features of the midbrain precursors (such as the expression of *Gad1* and *Gata3*) appear to be unaffected in the absence of Nkx2-2 or Skor2 function. This is in contrast to cerebellar Purkinje cells, in which Skor2 is required for the proper acquisition and maintenance of a GABAergic phenotype (Nakatani et al., 2014; Wang et al., 2011). In the midbrain, the pan-GABAergic features of the m2 precursors are likely controlled by the Gata/Tal TF complex (Achim et al., 2013; Kala et al., 2009). Nkx2-2 and Skor2 may regulate further neuronal subtype-specific characteristics, such as neurotransmitter reception, excitability, connectivity patterns, cellular morphology or co-neurotransmitter expression. Single-cell or cell-type specific RNA-sequencing could provide more information on the molecular composition of the *Nkx2-2*$^{+}$ *Skor2*$^{+}$ GABAergic neurons.

Skor2 as a putative marker of dMRF/vlPAG REM-off neurons

Interactions between REM-sleep promoting REM-on neurons in the dorsolateral pons and REM-sleep inhibiting REM-off neurons in the vlPAG/dMRF are thought to regulate normal sleep cycles (Luppi et al., 2017; Saper et al., 2010; Scammell et al., 2017; Weber and Dan, 2016). In rats, REM-sleep deprivation results in stimulation of dMRF/vlPAG GABAergic neurons, as evidenced by upregulation of the expression of the immediate-early gene *c-fos* (Sapin et al., 2009). A recent study of neuronal activity during sleep episodes demonstrated that dMRF/vlPAG GABAergic neurons increase their firing during transitions from non-REM sleep to wakefulness also in mice, consistent with the suggested REM-off activity (Weber et al., 2018). Optogenetic and chemogenetic activation of the dMRF/vlPAG GABAergic neurons decreases REM sleep, whereas their inhibition increases REM sleep (Hayashi et al., 2015; Weber et al., 2018). An important projection target of the inhibitory dMRF/vlPAG REM-off neurons is the dorsolateral pons, which contains excitatory glutamatergic REM-on neurons controlling both muscle atonia and other aspects of REM sleep. In turn, the regulatory inputs into the dMRF/vlPAG region include orexinergic excitatory projections from the ventral hypothalamus, which are implicated in the narcolepsy and narcolepsy-associated loss of muscle tone reminiscent of REM sleep (Kaur et al., 2009; Lu et al., 2006; Willie et al., 2003). The *Skor2*$^{+}$ neuron population described here appears to be integrated in this circuit in both directions.

Although their role in REM-sleep regulation is well established, the GABAergic neurons in the dMRF/vlPAG remain a heterogeneous population, containing cells of both REM-off and

Development (2022) 149, dev200937. doi:10.1242/dev.200937

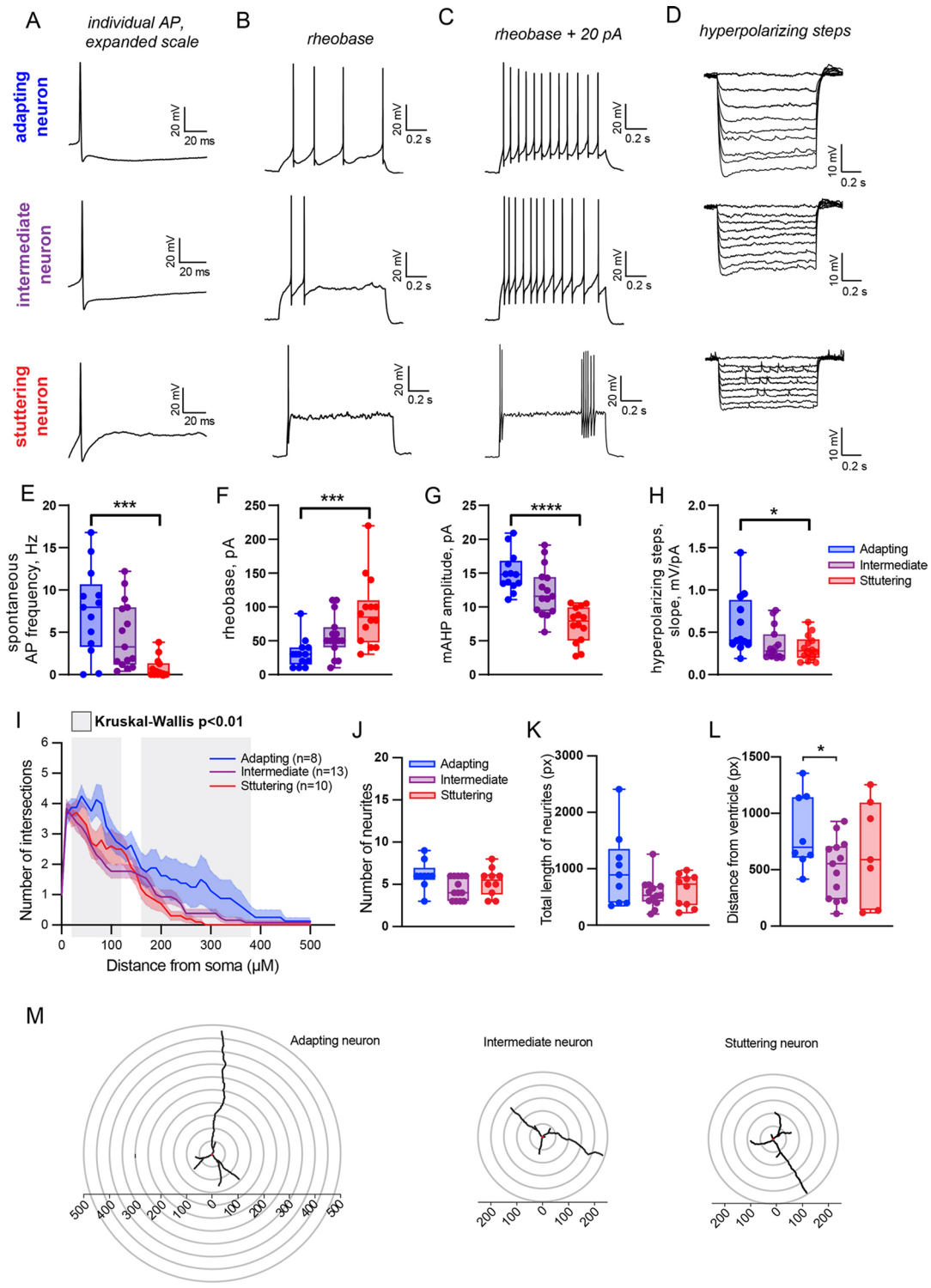

Fig. 7. Subtypes of dMRF/vlPAG *Skor2*$^{+}$ neurons with distinct electrophysiological and morphological characteristics. (A-D) Example traces of evoked action potential (AP) firing and voltage response to hyperpolarization in different types of GFP^{+} cells in the *Skor2*$^{GFP/+}$ mouse midbrain. (E-H) Excitability parameters of the GFP^{+} cells in the *Skor2*$^{GFP/+}$ mouse midbrain. Data are presented as individual values (dots) and box plot showing median, 25th and 75th percentiles with whiskers showing minimum and maximum values. mAHP, medium after-hyperpolarizing potential. Adapting cells *n*=13; intermediate cells *n*=15, and stuttering cells *n*=14, 17 animals. **P*<0.05; ****P*<0.001; *****P*<0.0001 (one-way ANOVA). (I) Sholl analysis comparing intermediate (*n*=8), adapting (*n*=13) and stuttering (*n*=10) subclass GFP+ cells in the *Skor2*$^{GFP/+}$ mouse midbrain for the number of intersections at a various distance from soma or cell body (16 animals). Data represented as mean±s.e.m. The gray shading indicates the region where the three groups show statistically significant differences (Kruskal–Wallis *P*<0.01). (J,K) Quantification of the neurite number (J) and total length of neurites (K) in adapting, intermediate and stuttering type of GFP^{+} neurons in the *Skor2*$^{GFP/+}$ mouse midbrain. Neurite number and total (summed) neurite length was calculated from the Sholl traced neurons. (L) Comparison of the distance of the cell soma from the midbrain ventricle in the three subclasses of GFP+ neurons in the *Skor2*$^{GFP/+}$ mouse midbrain. A difference between the means of distance from the ventricle was detected between adapting and intermediate neuron types (**P*<0.05; unpaired two-tailed *t*-test). (M) Reconstructions or tracing images of representative neurons used for Sholl analysis. The values are the distance from the neuronal soma (in μm).

Development (2022) 149, dev200937. doi:10.1242/dev.200937

REM-on activity (Luppi et al., 2017; Weber et al., 2018; Verret et al., 2006). We show here that the location of the *Skor2*-expressing dMRF/vlPAG cells matches the position of the REM-off neurons in the mouse and rat. Upregulation of c-Fos upon REM-sleep deprivation, projection to dorsolateral pons and responsiveness to orexin further support the hypothesis that at least some of the *Skor2*$^{+}$ cells represent dMRF/vlPAG REM-off neurons. Differences in the electrophysiology profiles and neuronal morphology of the *Skor2*-expressing neurons may indicate the presence of additional functional subclasses, which could have distinct roles in sleep regulation or other dMRF/vlPAG-mediated functions, such as non-REM sleep stages, eye and body movements, and nociception. Furthermore, our results show that, in addition to the *Skor2*-expressing neurons, the dMRF/vlPAG contains abundant other neurons that also project to the dorsolateral pontine area. Recording and modulation of the activity of the *Skor2*-expressing neurons during sleep behavior will be needed to unambiguously show their involvement in REM-sleep regulation. As the homozygous *Skor2* mutant mice die shortly after birth (Nakatani et al., 2014), conditional inactivation of *Skor2* in the midbrain will be needed to test the requirement of this TF for distinct subtype-specific anatomical and physiological properties of the dMRF/vlPAG GABAergic neurons.

Other cell types and functions of the MRF and PAG

In addition to the m2 derived *Skor2*-expressing GABAergic neurons described here, the MRF and PAG contain a variety of other cell types. Some of these are also involved in sleep regulation. For example, the vlPAG contains a group of neurotensin-expressing glutamatergic neurons that control non-REM sleep (Zhong et al., 2019). Furthermore, in addition to the GABAergic projection, the dMRF/vlPAG has been suggested to send glycinergic and glutamatergic projections to the dorsolateral pons, including the sublaterodorsal nucleus (Liang et al., 2014). Studies of the neuronal derivatives of the other embryonic midbrain regions, including the Nkx2-2-expressing GABAergic and glutamatergic precursors in the m4, potentially give insights into the molecular, anatomical and functional diversity of these neurons.

Our study of the developmental and molecular characteristics of the dMRF/vlPAG neurons illustrates that unique molecular markers of GABAergic neuron subtypes can be identified, and that such markers facilitate studying the function of specific neuronal circuits. Single-cell transcriptomic analyses would help to further dissect the heterogeneity of the developing midbrain region and the neuronal circuits therein.

MATERIALS AND METHODS

Mouse lines

En1^{Cre} (Kimmel et al., 2000), *Gad67*^{GFP} (Tamamaki et al., 2003), *Gata2*^{flox} (Haugas et al., 2010), *Ai14*^{TdTomato} (Madisen et al., 2010) were maintained on an outbred (ICR) background and *Nkx2-2*^{Cre} (Balderes et al., 2013) and *Skor2*^{GFP} (Nakatani et al., 2014) alleles were maintained on a mixed background (C57BL/6 and ICR). E0.5 was defined as noon of the day of the vaginal plug. Experiments were approved by the Laboratory Animal Center, University of Helsinki, and the National Animal Experiment Board in Finland.

Microarrays

Ventral and dorsal midbrain was dissected from E12.5 wild-type and *Gata2*^{cko} (Kala et al., 2009) embryos. For both genotypes, three sample pools were generated, each consisting of six tissue samples. Total RNA was extracted with Trizol reagent and used for probe labeling. Illumina BeadChip (Mouse WG-6 2.0) microarrays were hybridized according to the manufacturer's protocol. The dataset was normalized using the quantile normalization method. Statistical testing was performed using LIMMA package using R and Bioconductor statistical analysis software. DAVID Bioinformatics Resources 6.7 [National Institute of Allergy and Infectious Diseases/National Institutes of Health (NIH); Huang da et al., 2009a,b] were used for the GO term enrichment analyses.

Histology, mRNA *in situ* hybridization and immunohistochemistry

Dissected embryos, or brain tissue from embryos older than E16, were fixed in 4% paraformaldehyde (PFA; Sigma-Aldrich, P6148) in PBS. To collect adult mouse and rat brains, intracardial perfusion was performed with PBS and 4% PFA. Brains were dissected and fixed in 4% PFA. For paraffin embedding and microtome sectioning, samples were transferred to Histosec polymer wax (Merck Millipore) and sectioned at 5 or 10 µm. For vibratome sectioning, adult mouse brain tissue samples were embedded in 4% agarose and sections were cut using a Leica VT1200S vibratome. Vibratome sections were stored in ice-cold 1×PBS until further processing. mRNA ISH was performed using digoxigenin (DIG)-labeled antisense cRNA probes. For ISH signal detection, we used the tyramide signal amplification (TSA)-based method (TSA Plus Cy3 NEL744001KT/Fluorescein NEL741001KT; Perkin Elmer) for fluorescent detection or the alkaline phosphatase (AP)-based method for colorimetric detection [Wilkinson and Green, 1990 (with modifications)].

For combined ISH and IHC, ISH signal was visualized first, followed by the IHC protocol. For double ISH, DIG- and fluorescein-labeled probes were combined. TSA Plus Cyanine 3 and Fluorescein kits were used for detection. Antibodies and mRNA ISH probes are listed in Table S5.

For the rat Skor2 probe, the rat Skor2 cDNA fragment (GeneArt sequence-based gene synthesis, Life Technologies) was cloned into a pBluescript SK+ vector digested with NotI and SalI. The plasmid map and sequence are available upon request. All analyses were performed using at least three biological replicates.

Stereotaxic injections and retrograde tracing

Mice used in the experiments were *Skor2*$^{GFP/wt}$ (n=6). Mice were anesthetized with isoflurane, attached to the stereotaxic frame, and a small hole was drilled into the skull. For retrograde tracing of vlPAG neurons, bilateral intracranial injections of 0.2% CtB subunit (#104; List Biological Lab) were injected at the speed of 50 nl/min using a microinjector (UltraMicroPump III, World Precision Instruments) and microsyringe (Hamilton, 7803-06). The stereotaxic coordinates for injections were (measured from bregma, in mm): −5.19 to −5.4 (AP); 0.88 (ML); −4.4 (DV). The coordinates were obtained from the mouse brain atlas (Paxinos and Franklin, 2012). Mice were intracardially perfused 5-7 days after the injections and the brains were collected. Brains were sectioned using a vibratome. IHC was performed using anti-GFP and anti-CtB antibodies (Table S5). The quantification was performed by counting the number of cells labeled with DAPI, CtB, GFP and both GFP and CtB in the dMRF/vlPAG area. The statistical analyses were performed using R.

REM-sleep deprivation assay in rats

The REM sleep of male Han-Wistar rats was deprived for 72 h as described previously (Porkka-Heiskanen et al., 1995) using the water tank (inverted flowerpot) method, when the animal has to sleep on a small platform surrounded by water. The platform is so small that the animal is not able to maintain its balance on it during the REM-sleep-associated muscle hypotonia and falls into the water, thus REM sleep is suppressed almost totally.

Small platforms (inverted flowerpots, diameter: 6.5 cm) were placed into a round shape wire mesh cage situated in a basin. The wire mesh cage was provided with food tubes and water bottles. All animals were kept in a 12 h:12 h light-dark cycle (light was on from 8:30-20:30) before and during the experiment. Before the REM-sleep deprivation, the rats were placed into the dry apparatus (water tank) for 48 h in order to adapt them to the new environment. Then the basin was filled with water for 72 h. Simultaneously,

Development (2022) 149, dev200937. doi:10.1242/dev.200937

three rats were placed into the wire mesh cage with four platforms. The animals had food and water *ad libitum*. The rats of the two control groups (LPC: large, 11-cm-diameter platforms were placed into the basin filled with water, the platforms were large enough to have REM sleep on them; DC: there was no water in the basin with platforms, bedding was placed on the bottom) were kept in the apparatus for the corresponding time (48+72 h). An additional group of rats was allowed to have 9 h recovery sleep after the 72-h REM-sleep deprivation (REMSD+Rec group). The REM-sleep deprivation of DC, LPC and REMSD rats started and ended 20-40 min before dark onset. The REM-sleep deprivation of REMSD+Rec group started end ended 9 h earlier (9 h 20-40 min before dark onset, i.e. 2 h 20-40 min after light onset). At the end of the REM-sleep deprivation/sham deprivation or rebound sleep, the animals were sacrificed by intraperitoneal administration of 400 mg/kg chloral hydrate, perfused with PBS and then with 4% PFA, and the brains were removed for histochemical examination and for measuring gene expression.

For quantification of the c-Fos labeling, sections covering the dMRF/vlPAG area were collected from all REM-sleep assay animals and stained for the expression of c-Fos (IHC) and *Skor2* (ISH). The number of *Skor2*$^{+}$ cells and the number of *Skor2*$^{+}$ cells double labeled with c-Fos were counted (Table S4).

This study contained two similar yet separate experiment series. These experiment series, while experiment design was identical, were conducted at different times. We observed a systematic difference in c-Fos staining efficiency between experiment series (Fig. S7). To alleviate this difference, we performed *z*-score transformation to get experiment series on the same scale. The scaled data was pooled before multiple comparison between groups. The number of animals in each group was: n=6 for REMSD, n=5 in the DC, n=6 in LPC and n=3 in REMSD+Rec group. The number of *Skor2*$^{+}$ cells did not appear to vary between the experiments (*Skor2*$^{+}$ cells; 72±28). Kruskal–Wallis test for multiple comparison was used to test the variation in the mean transformed *z*-scores between all the experiment groups (experiment series merged). Pairwise group comparisons (experiment series merged) were performed using the Wilcox-test. The group identity, experiment ID, number of *Skor2*$^{+}$ cells, number of c-Fos^{+} cells, the percent of c-Fos labeled *Skor2*$^{+}$ cells and the transformed *z*-scores for each animal can be found in Table S4.

Electrophysiology

Adult *Skor2*$^{GFP/+}$ mice of both genders (2-7 months old, n=27) were used for the preparation of acute brain slices. Animals were anesthetized with isoflurane. After decapitation, the brain was rapidly removed and transferred to ice-cold cutting solution containing 92 mM NMDG, 2.5 mM KCl, 1.25 mM NaH_2PO_4, 30 mM $NaHCO_3$, 20 mM HEPES, 25 mM glucose, 2 mM thiourea, 5 mM Na-ascorbate, 3 mM Na-pyruvate, 0.5 mM $CaCl_2$ and 10 mM $MgSO_4$ (pH 7.3-7.4 was adjusted with concentrated hydrochloric acid). All extracellular solutions were equilibrated with 95% O_2 and 5% CO_2. Coronal slices (250 µm) containing the dMRF/vlPAG were cut using a vibrating microtome (7000 SMZ-2; Campden Instruments). Slices were kept for 10 min in NMDG cutting solution at 34°C before being transferred to recovery solution (at room temperature) containing 92 mM NaCl, 2.5 mM KCl, 1.25 mM NaH_2PO_4, 30 mM $NaHCO_3$, 20 mM HEPES, 25 mM glucose, 2 mM thiourea, 5 mM Na-ascorbate, 3 mM Na-pyruvate, 2 mM $CaCl_2$ and 2 mM $MgSO_4$. Recordings were carried out 1-5 h after the preparation of acute slices. Whole-cell patch clamp recordings from visually identified dMRF/vlPAG cells (GFP^{+} cells and neighboring GFP^{-} cells as control) were performed in a submerged recording chamber at 32±0.5°C, constantly perfused with ACSF [124 mM NaCl, 3 mM KCl, 2 mM $CaCl_2$, 26 mM $NaHCO_3$, 1.25 mM NaH_2PO_4, 1 mM $MgSO_4$ and 15 mM glucose (pH 7.4). Bath perfusion was 2.5 ml min^{-1}]. Application of orexin A (1 µM, Tocris) and elevated K^{+} was done using a direct perfusion system locally onto the slice.

Whole-cell current-clamp recordings were obtained using a Multiclamp 700 A patch-clamp amplifier and recorded with pClamp 10 (Molecular Devices) at a sampling rate of 20-50 kHz. Borosilicate patch pipette resistance ranged from 3 to 6 MΩ. The composition of the patch pipette solution was: 135 mM K-gluconate, 10 mM HEPES, 5 mM EGTA, 4 mM Mg-ATP, 0.5 mM Na-GTP, 2 mM KCl, 2 mM $Ca(OH)_2$, 280 mM mOsm (pH 7.2). The liquid junction potential of 13 mV was not corrected for. In some experiments biocytin (7 mM, Sigma-Aldrich) was included in the pipette solution to allow post hoc staining of the recorded cells.

For characterization of the cell properties, the cells were held in current clamp at −70 mV, and we injected hyperpolarizing and depolarizing current steps (1 s, increment of 10 pA). Excitability parameters were analyzed with the FFFPA script in Matlab (https://doi.org/10.5281/zenodo.3667731), except for the mAHP amplitude and hyperpolarizing steps. The mAHP amplitude was measured in Clampfit 11.1 as the mean voltage 15-20 ms after the AP threshold. The voltage response to current hyperpolarizing steps was measured in Clampfit 11.1. The hyperpolarizing steps slope was calculated by linear fit of voltage response amplitude plotted against the injected current. The effect of orexin A on cells was assessed in the voltage clamp. Cells were held at −70 mV and test pulses (−10 mV, 50 ms) were delivered every minute to monitor access resistance. The change in holding current was measured after 1 min of orexin A application. For counting the number of cells which responded to orexin application, the threshold for orexin-evoked response was set at the level of baseline root mean square noise multiplied by two. Placement of direct perfusion tubing was verified by application of 8 mM KCl at the end of experiment. The analysis of electrophysiological recordings was carried out using Clampfit 11.1 (Molecular Devices) and Matlab, and GraphPad Prism 9 was used for statistical analysis.

Sholl analysis of neuronal morphology by biocytin filling

Biocytin-filled GABAergic neurons from the dMRF/vlPAG region were immunohistochemically stained and imaged using a Leica SP8 STED confocal microscope. Tiled confocal *z*-stack images (40 images/stack) were acquired at 20× objective. Sholl analysis was performed as previously described (Comhair et al., 2018). Briefly, 8-bit images of dMRF/vlPAG GABAergic neurons were traced using the Simple Neurite Tracer (SNT v3.2.14) (Arshadi et al., 2021) plug-in of FIJI and tracing files were generated. The number of dendrites and total dendrite length were generated using the measurement function of Simple Neurite Tracer. The complexity of the neurites was evaluated using the Sholl analysis. To implement this, concentric sampling spheres with 10 µm intervals between the radii were formed around the central point, i.e. the soma of the traced neuron, and a number of intersections with neurites were measured. Comparative analysis of Sholl curves between neuron types was made using a Kruskal–Wallis test within a 50 µm wide moving window. Separate pairwise comparison between Sholl curves of neuron types was carried out using a Kolmogorov–Smirnov test within a 50 µm wide moving window. Distance intervals with a statistically significant difference between the curves were indicated (P-value <0.01, shaded areas in Fig. 7I). Distance from ventricle per biocytin-filled neuron types was measured in pixels and the cell groups compared by unpaired two-tailed *t*-test. Normality of the distance distribution was tested with Shapiro before conducting the *t*-test. Statistical analyses were performed in GraphPad Prism 9 and R.

Acknowledgements

We thank Outi Kostia and Eija Koivunen for expert technical assistance. We thank Wolfgang Wurst for the *En1*^{Cre} and Lori Sussel for the *Nkx2-2*^{Cre} mice. We acknowledge the DNA Microarray Centre at Turku Centre for Biotechnology and Matti Kankainen and Daniel Borshagovski for help in gene expression profiling and data analyses.

Competing interests

The authors declare no competing or financial interests.

Author contributions

Conceptualization: K.A., L.L., A.K., M.S., T.S., J.P.; Methodology: A.K., P. Singh, L.L., P. Seja, Z.L., A.M., S.K., T.S., S.M., T.A.-A.; Software: S.K.; Validation: A.K., P. Singh, L.L., Z.L., A.M., S.M., T.A.-A.; Formal analysis: K.A., A.K., P. Singh, P. Seja, Z.L., A.M., S.K., S.M., J.P.; Investigation: K.A., A.K., P. Singh, L.L., P. Seja, Z.L., A.M., S.K., M.S., T.S., S.M., J.P., T.A.-A.; Resources: Z.L., Y.O., M.S., T.S., S.M., J.P., T.A.-A.; Data curation: K.A., A.K., P. Singh, S.K., T.S., S.M., J.P.; Writing - original draft: K.A., A.K., P. Singh, L.L., Z.L., S.K., Y.O., M.S., T.S., S.M., J.P., T.A.-A.; Writing - review & editing: K.A., L.L., J.P., T.A.-A.; Visualization: K.A., A.K., P. Singh, L.L., P. Seja, S.K., S.M.; Supervision: K.A., M.S., T.S., S.M., J.P., T.A.-A.; Project administration: K.A., T.S., J.P.; Funding acquisition: J.P.

Funding
This paper was supported by Academy of Finland; Sigrid Juséliuksen Säätiö; Jane ja Aatos Erkon Säätiö; Magnus Ehrnroothin Säätiö.

Data availability
Microarray data have been deposited in GEO under accesssion number GSE208110.

Peer review history
The peer review history is available online at https://journals.biologists.com/dev/article-lookup/doi/10.1242/dev.200937

References

Achim, K., Peltopuro, P., Hui-Hsin, T., Zachariah, A., Åstrand, M., Rowitch, D., Salminen, M. and Partanen, J. (2013). The role of Tal2 and Tal1 in the differentiation of midbrain GABAergic neuron precursors. *Biol. Open* **2**, 990-997. doi:10.1242/bio.20135041

Arshadi, C., Günther, U., Eddison, M., Harrington, K. I. S. and Ferreira, T. A. (2021). SNT: a unifying toolbox for quantification of neuronal anatomy. *Nat. Methods* **18**, 374-377. doi:10.1038/s41592-021-01105-7

Balderes, D. A., Magnuson, M. A. and Sussel, L. (2013). Nkx2.2:Cre knock-in mouse line: a novel tool for pancreas- and CNS-specific gene deletion. *Genesis* **51**, 844-851. doi:10.1002/dvg.22715

Boissard, R., Fort, P., Gervasoni, D., Barbagli, B. and Luppi, P. H. (2003). Localization of the GABAergic and non-GABAergic neurons projecting to the sublaterodorsal nucleus and potentially gating paradoxical sleep onset. *Eur. J. Neurosci.* **18**, 1627-1639. doi:10.1046/j.1460-9568.2003.02861.x

Chlon, T. M. and Crispino, J. D. (2012). Combinatorial regulation of tissue specification by GATA and FOG factors. *Development* **139**, 3905-3916. doi:10.1242/dev.080440

Comhair, J., Devoght, J., Morelli, G., Harvey, R. J., Briz, V., Borrie, S. C., Bagni, C., Rigo, J. M., Schiffmann, S. N., Gall, D. et al. (2018). Alpha2-containing glycine receptors promote neonatal spontaneous activity of striatal medium spiny neurons and support maturation of glutamatergic inputs. *Front. Mol. Neurosci.* **11**, 380. doi:10.3389/fnmol.2018.00380

Guimera, J., Weisenhorn, D. V. and Wurst, W. (2006). Megane/Heslike is required for normal GABAergic differentiation in the mouse superior colliculus. *Development* **133**, 3847-3857. doi:10.1242/dev.02557

Haugas, M., Lillevali, K., Hakanen, J. and Salminen, M. (2010). Gata2 is required for the development of inner ear semicircular ducts and the surrounding perilymphatic space. *Dev. Dyn.* **239**, 2452-2469. doi:10.1002/dvdy.22373

Hayashi, Y., Kashiwagi, M., Yasuda, K., Ando, R., Kanuka, M., Sakai, K. and Itohara, S. (2015). Cells of a common developmental origin regulate REM/non-REM sleep and wakefulness in mice. *Science* **350**, 957-961. doi:10.1126/science.aad1023

Huang da, W., Sherman, B. T. and Lempicki, R. A. (2009a). Bioinformatics enrichment tools: paths toward the comprehensive functional analysis of large gene lists. *Nucleic Acids Res.* **37**, 1-13. doi:10.1093/nar/gkn923

Huang da, W., Sherman, B. T. and Lempicki, R. A. (2009b). Systematic and integrative analysis of large gene lists using DAVID bioinformatics resources. *Nat. Protoc.* **4**, 44-57. doi:10.1038/nprot.2008.211

Kala, K., Haugas, M., Lilleväli, K., Guimera, J., Wurst, W., Salminen, M. and Partanen, J. (2009). Gata2 is a tissue-specific post-mitotic selector gene for midbrain GABAergic neurons. *Development* **136**, 253-262. doi:10.1242/dev.029900

Kaur, S., Thankachan, S., Begum, S., Liu, M., Blanco-Centurion, C. and Shiromani, P. J. (2009). Hypocretin-2 saporin lesions of the ventrolateral periaquaductal gray (vlPAG) increase REM sleep in hypocretin knockout mice. *PLoS One* **4**, e6346. doi:10.1371/journal.pone.0006346

Keay, K. A. and Bandler, R. (2001). Parallel circuits mediating distinct emotional coping reactions to different types of stress. *Neurosci. Biobehav. Rev.* **25**, 669-678. doi:10.1016/S0149-7634(01)00049-5

Kimmel, R. A., Turnbull, D. H., Blanquet, V., Wurst, W., Loomis, C. A. and Joyner, A. L. (2000). Two lineage boundaries coordinate vertebrate apical ectodermal ridge formation. *Genes Dev.* **14**, 1377-1389.

Lahti, L., Haugas, M., Tikker, L., Airavaara, M., Voutilainen, M. H., Anttila, J., Kumar, S., Inkinen, C., Salminen, M. and Partanen, J. (2016). Differentiation and molecular heterogeneity of inhibitory and excitatory neurons associated with midbrain dopaminergic nuclei. *Development* **143**, 516-529. doi:10.1242/dev.129957

Liang, C. L., Quang Nguyen, T. and Marks, G. A. (2014). Inhibitory and excitatory amino acid neurotransmitters are utilized by the projection from the dorsal deep mesencephalic nucleus to the sublaterodorsal nucleus REM sleep induction zone. *Brain Res.* **1567**, 1-12. doi:10.1016/j.brainres.2014.04.016

Lillevali, K., Matilainen, T., Karis, A. and Salminen, M. (2004). Partially overlapping expression of Gata2 and Gata3 during inner ear development. *Dev. Dyn.* **231**, 775-781. doi:10.1002/dvdy.20185

Lu, J., Sherman, D., Devor, M. and Saper, C. B. (2006). A putative flip-flop switch for control of REM sleep. *Nature* **441**, 589-594. doi:10.1038/nature04767

Luppi, P. H., Peyron, C. and Fort, P. (2017). Not a single but multiple populations of GABAergic neurons control sleep. *Sleep Med. Rev.* **32**, 85-94. doi:10.1016/j.smrv.2016.03.002

Madisen, L., Zwingman, T. A., Sunkin, S. M., Oh, S. W., Zariwala, H. A., Gu, H., Ng, L. L., Palmiter, R. D., Hawrylycz, M. J., Jones, A. R. et al. (2010). A robust and high-throughput Cre reporting and characterization system for the whole mouse brain. *Nat. Neurosci.* **13**, 133-140. doi:10.1038/nn.2467

Makrides, N., Panayiotou, E., Fanis, P., Karaiskos, C., Lapathitis, G. and Malas, S. (2018). Sequential role of SOXB2 factors in GABAergic neuron specification of the dorsal midbrain. *Front. Mol. Neurosci.* **11**, 152. doi:10.3389/fnmol.2018.00152

Morello, F., Borshagovski, D., Survila, M., Tikker, L., Sadik-Ogli, S., Kirjavainen, A., Estartus, N., Knaapi, L., Lahti, L., Törönen, P. et al. (2020). Molecular fingerprint and developmental regulation of the tegmental GABAergic and glutamatergic neurons derived from the anterior hindbrain. *Cell Rep.* **33**, 108268. doi:10.1016/j.celrep.2020.108268

Nakatani, T., Minaki, Y., Kumai, M. and Ono, Y. (2007). Helt determines GABAergic over glutamatergic neuronal fate by repressing Ngn genes in the developing mesencephalon. *Development* **134**, 2783-2793. doi:10.1242/dev.02870

Nakatani, T., Minaki, Y., Kumai, M., Nitta, C. and Ono, Y. (2014). The c-Ski family member and transcriptional regulator Corl2/Skor2 promotes early differentiation of cerebellar Purkinje cells. *Dev. Biol.* **388**, 68-80. doi:10.1016/j.ydbio.2014.01.016

Paxinos, G. and Franklin, K. (2012). *Paxinos and Franklin's the Mouse Brain in Stereotactic Coordinates*, 4th edn. Academic Press.

Porkka-Heiskanen, T., Smith, S. E., Taira, T., Urban, J. H., Levine, J. E., Turek, F. W. and Stenberg, D. (1995). Noradrenergic activity in rat brain during rapid eye movement sleep deprivation and rebound sleep. *Am. J. Physiol.* **268**, R1456-R1463. doi:10.1152/ajpregu.1995.268.6.R1456

Prakash, N., Puelles, E., Freude, K., Trumbach, D., Omodei, D., Di Salvio, M., Sussel, L., Ericson, J., Sander, M., Simeone, A. et al. (2009). Nkx6-1 controls the identity and fate of red nucleus and oculomotor neurons in the mouse midbrain. *Development* **136**, 2545-2555. doi:10.1242/dev.031781

Puelles, E., Annino, A., Tuorto, F., Usiello, A., Acampora, D., Czerny, T., Brodski, C., Ang, S. L., Wurst, W. and Simeone, A. (2004). Otx2 regulates the extent, identity and fate of neuronal progenitor domains in the ventral midbrain. *Development* **131**, 2037-2048. doi:10.1242/dev.01107

Saper, C. B., Fuller, P. M., Pedersen, N. P., Lu, J. and Scammell, T. E. (2010). Sleep state switching. *Neuron* **68**, 1023-1042. doi:10.1016/j.neuron.2010.11.032

Sapin, E., Lapray, D., Bérod, A., Goutagny, R., Léger, L., Ravassard, P., Clément, O., Hanriot, L., Fort, P. and Luppi, P. H. (2009). Localization of the brainstem GABAergic neurons controlling paradoxical (REM) sleep. *PLoS One* **4**, e4272. doi:10.1371/journal.pone.0004272

Scammell, T. E., Arrigoni, E. and Lipton, J. O. (2017). Neural circuitry of wakefulness and sleep. *Neuron* **93**, 747-765. doi:10.1016/j.neuron.2017.01.014

Tamamaki, N., Yanagawa, Y., Tomioka, R., Miyazaki, J., Obata, K. and Kaneko, T. (2003). Green fluorescent protein expression and colocalization with calretinin, parvalbumin, and somatostatin in the GAD67-GFP knock-in mouse. *J. Comp. Neurol.* **467**, 60-79. doi:10.1002/cne.10905

Tikker, L., Casarotto, P., Singh, P., Biojone, C., Piepponen, T. P., Estartús, N., Seelbach, A., Sridharan, R., Laukkanen, L., Castrén, E. et al. (2020). Inactivation of the GATA cofactor ZFPM1 results in abnormal development of dorsal raphe serotonergic neuron subtypes and increased anxiety-like behavior. *J. Neurosci.* **40**, 8669-8682. doi:10.1523/JNEUROSCI.2252-19.2020

Wang, B., Harrison, W., Overbeek, P. A. and Zheng, H. (2011). Transposon mutagenesis with coat color genotyping identifies an essential role for Skor2 in sonic hedgehog signaling and cerebellum development. *Development* **138**, 4487-4497. doi:10.1242/dev.067264

Weber, F. and Dan, Y. (2016). Circuit-based interrogation of sleep control. *Nature* **538**, 51-59. doi:10.1038/nature19773

Weber, F., Hoang Do, J. P., Chung, S., Beier, K. T., Bikov, M., Saffari Doost, M. and Dan, Y. (2018). Regulation of REM and non-REM sleep by periaqueductal GABAergic neurons. *Nat. Commun.* **9**, 354. doi:10.1038/s41467-017-02765-w

Verret, L., Fort, P., Gervasoni, D., Léger, L. and Luppi, P. H. (2006). Localization of the neurons active during paradoxical (REM) sleep and projecting to the locus coeruleus noradrenergic neurons in the rat. *J. Comp. Neurol.* **495**, 573-586. doi:10.1002/cne.20891

Wilkinson, D. G. and Green, J. (1990). In situ hybridization and the three-dimensional construction of serial sections. In *Postimplantation Mammalian Embryos* (ed. A. J. Copp and D. L. Cockroft), pp. 155-171. Oxford, UK: Oxford University Press.

Willie, J. T., Chemelli, R. M., Sinton, C. M., Tokita, S., Williams, S. C., Kisanuki, Y. Y., Marcus, J. N., Lee, C., Elmquist, J. K., Kohlmeier, K. A.

et al. (2003). Distinct narcolepsy syndromes in Orexin receptor-2 and Orexin null mice: molecular genetic dissection of non-REM and REM sleep regulatory processes. *Neuron* **38**, 715-730. doi:10.1016/S0896-6273(03)00330-1

Virolainen, S.-M., Achim, K., Peltopuro, P., Salminen, M. and Partanen, J. (2012). Transcriptional regulatory mechanisms underlying the GABAergic neuron fate in different diencephalic prosomeres. *Development* **139**, 3795-3805. doi:10.1242/dev.075192

Zhong, P., Zhang, Z., Barger, Z., Ma, C., Liu, D., Ding, X. and Dan, Y. (2019). Control of non-REM sleep by midbrain neurotensinergic neurons. *Neuron* **104**, 795-809.e6. doi:10.1016/j.neuron.2019.08.026

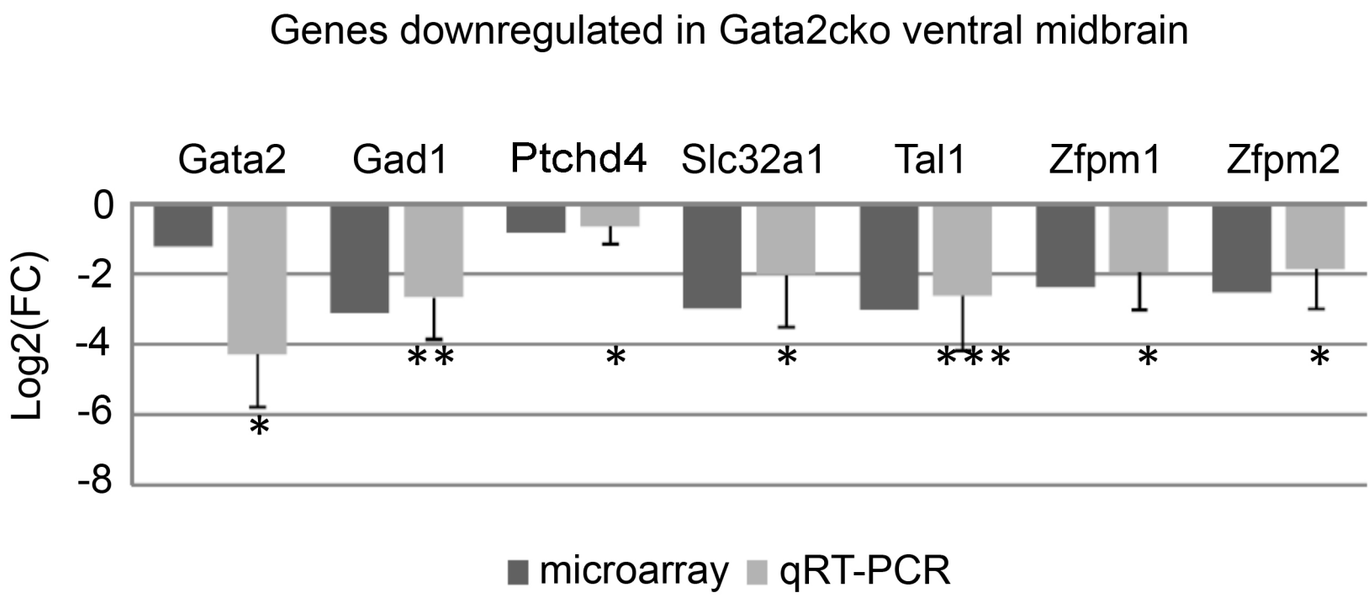

Fig. S1. Comparison of the fold change indicated by the microarray data analysis and quantitative RT-PCR. FC, fold change. For a selection of predicted Gata2-regulated genes, qRT-PCR assay was performed. After RT-PCR, fold change was calculated using the Ct values detected in the *Gata2*^{cko} and control (*En1*^{Cre}*; Gata2*$^{flox/wt}$) cDNA. Samples were normalized against *Actb* expression level in the same sample. The qRT-PCR was performed with 4 replicate cDNA samples. The statistical significance of the fold change in normalized expression levels is indicated. *** P<0.001, ** P<0.01, * P<0.05. The results of the microarray and qRT-PCR are largely consistent. An exception is the *Gata2* gene, where the microarray detects a truncated non-functional transcript.

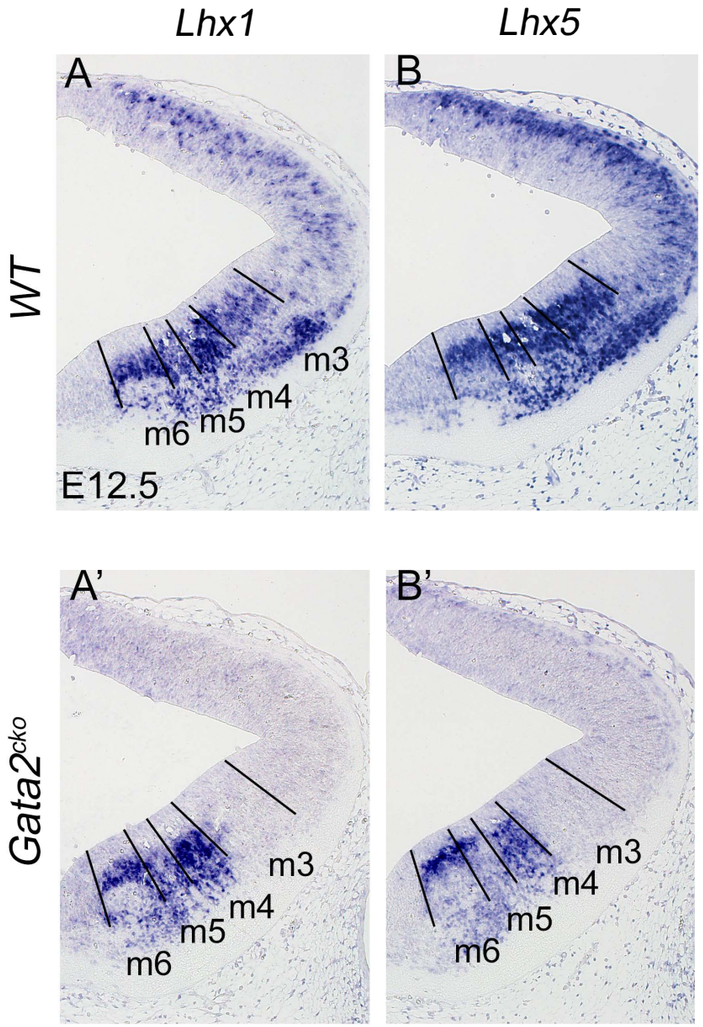

Fig. S2. ISH analysis. (A-B') Lhx1 (A,A') and Lhx5 (B,B') in wild-type and Gata2cko mutant embryos at E12.5.

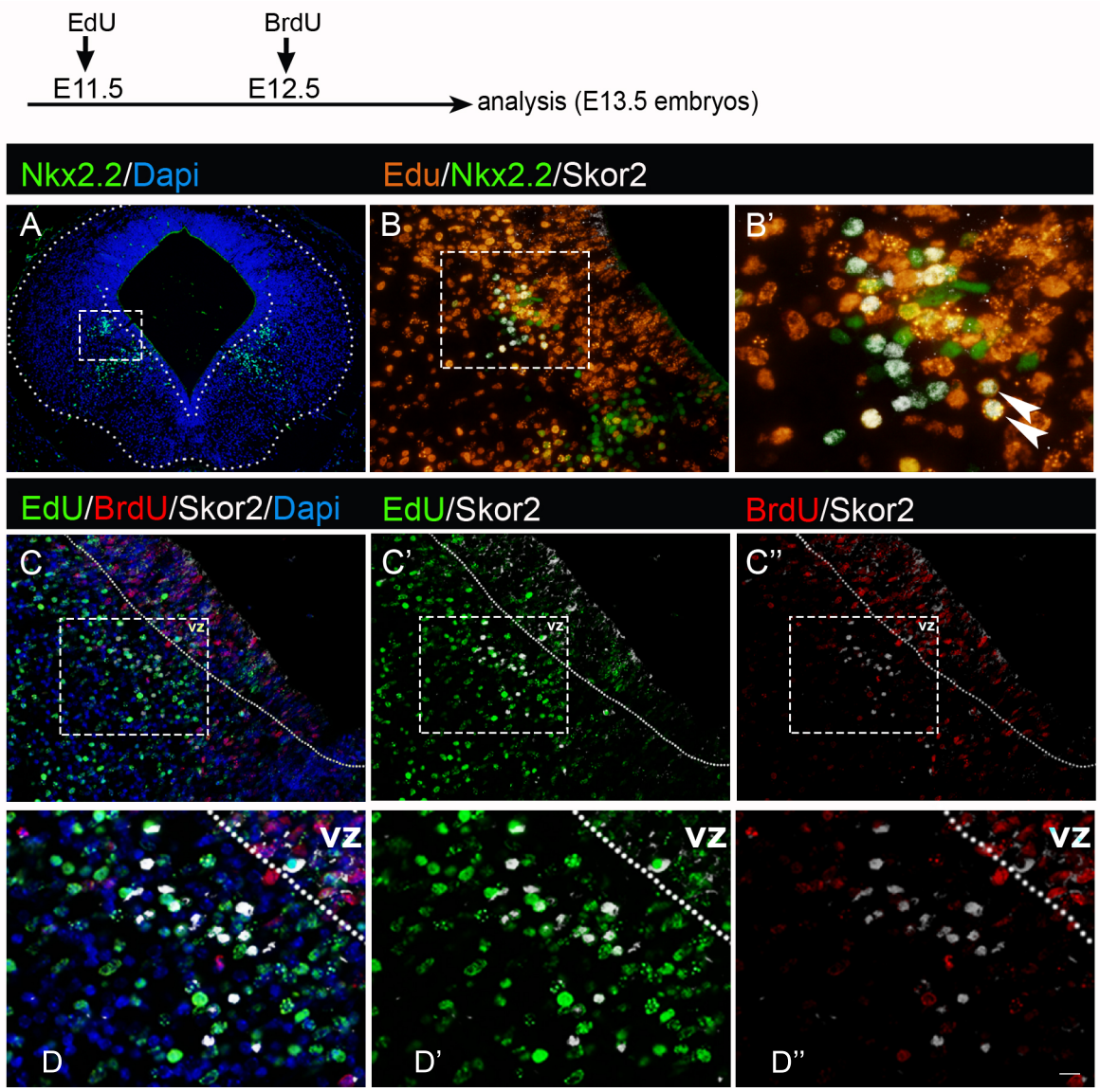

Fig. S3. *Skor2*$^{+}$ neuron birth-dating by BrdU and EdU labelling.

Pregnant females received one dose of EdU at E11.5 and one dose of BrdU at E12.5 of pregnancy. Embryos were dissected at E13.5 and analyzed for the label.

A, Nkx2-2 IHC on a coronal section of the E13.5 mouse midbrain.

B-B', Coexpression of Nkx2-2, Skor2 and EdU in E13.5 mouse midbrain. B', a close-up of Skor2^{+} cells (dashed box in B). Arrowheads indicate triple-labelled cells.

C-D'', Labelling for EdU and BrdU in Skor2^{+} cells. EdU is detected in most of the Skor2^{+} cells (C'). BrdU is not detected in the Skor2^{+} cells (C''). Close-ups of indicated regions are shown in D-D''. vz, ventricular zone.

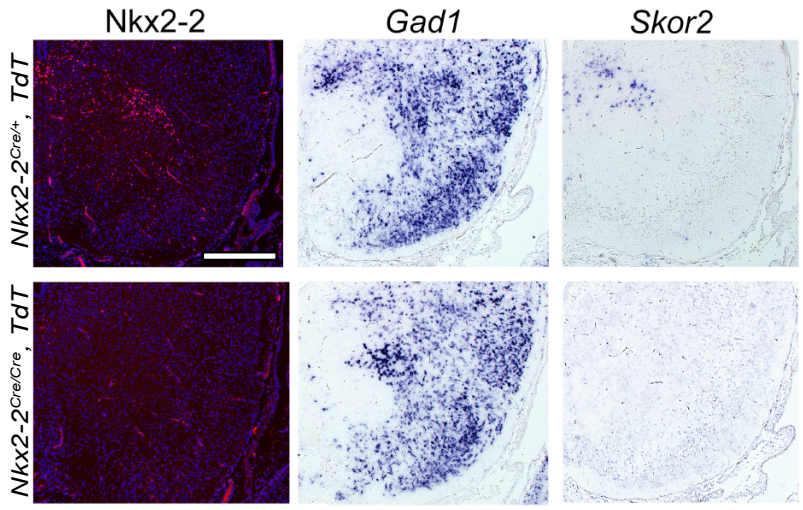

Fig. S4. *Skor2*, but not *Gad1* expression is lost in the *Nkx2-2* mutant mouse.

Coronal sections of E18.5 mouse midbrain analysed for the expression of Nkx2-2 (IHC), *Gad1* and *Skor2* (ISH), in *Ctrl* (*Nkx2-2*$^{Cre/wt}$, *TdT*) and *Nkx2-2*^{null} mutant (*Nkx2-2*$^{Cre/Cre}$, *TdT)* mice. Scale bar: 200 μm.

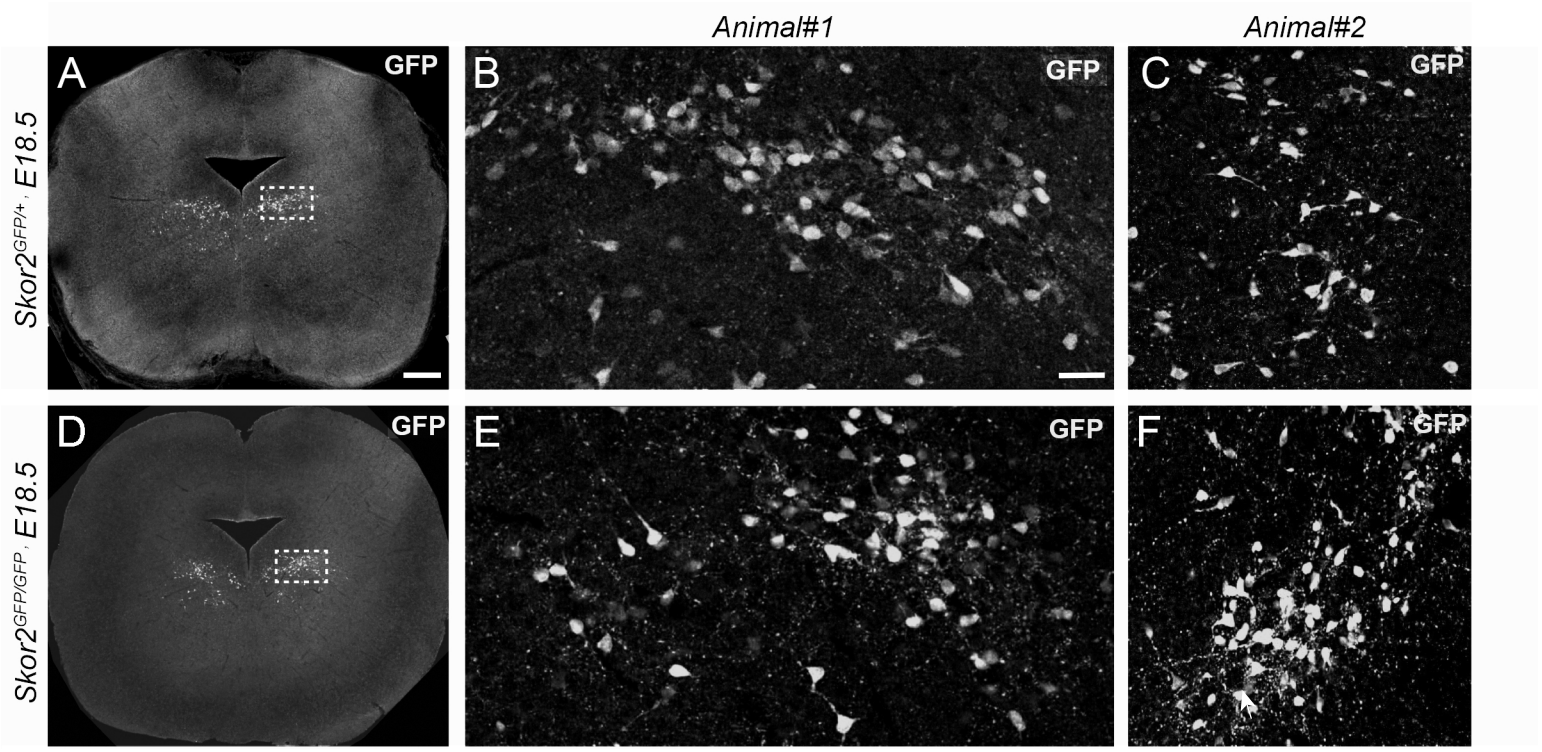

Fig. S5. Normal appearance of neurons expressing the *Skor2* gene is in mice homozygous for a *Skor2* null allele. GFP expression (IHC) on coronal sections of E18.5 *Skor2*$^{GFP/+}$ (A-C) and *Skor2*$^{GFP/GFP}$ midbrain (D-F). The position and number of cells as well as the number and appearance of neurites look similar between the genotypes. Arrowheads point to neuronal projections. Scale bar: 200 μm (A,D), 50 μm (B,C,E,F).

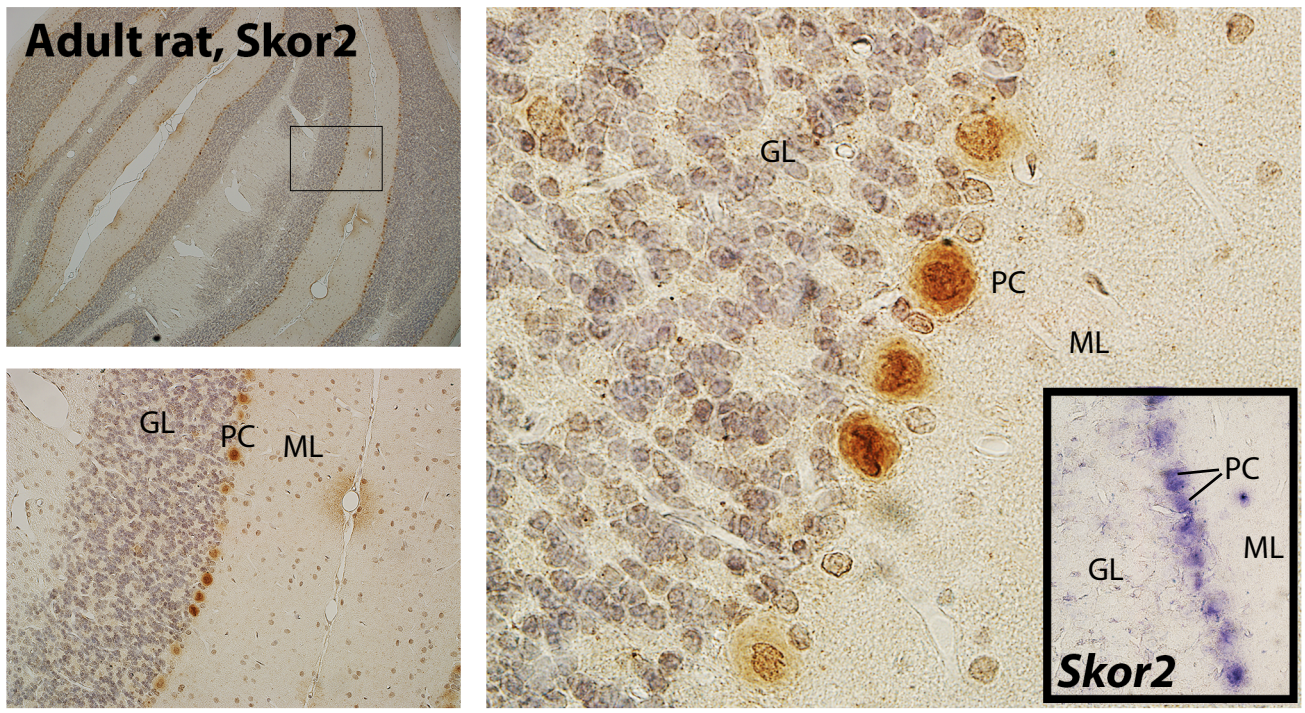

Fig. S6. Skor2 expression in the adult rat cerebellum. IHC and ISH on coronal sections. Skor2 protein was detected in the Purkinje cells (PC) in the rat cerebellum (orange, IHC). The inset shows *Skor2* mRNA expression in the Purkinje cells (violet, ISH). ML, molecular layer; GC, granular layer.

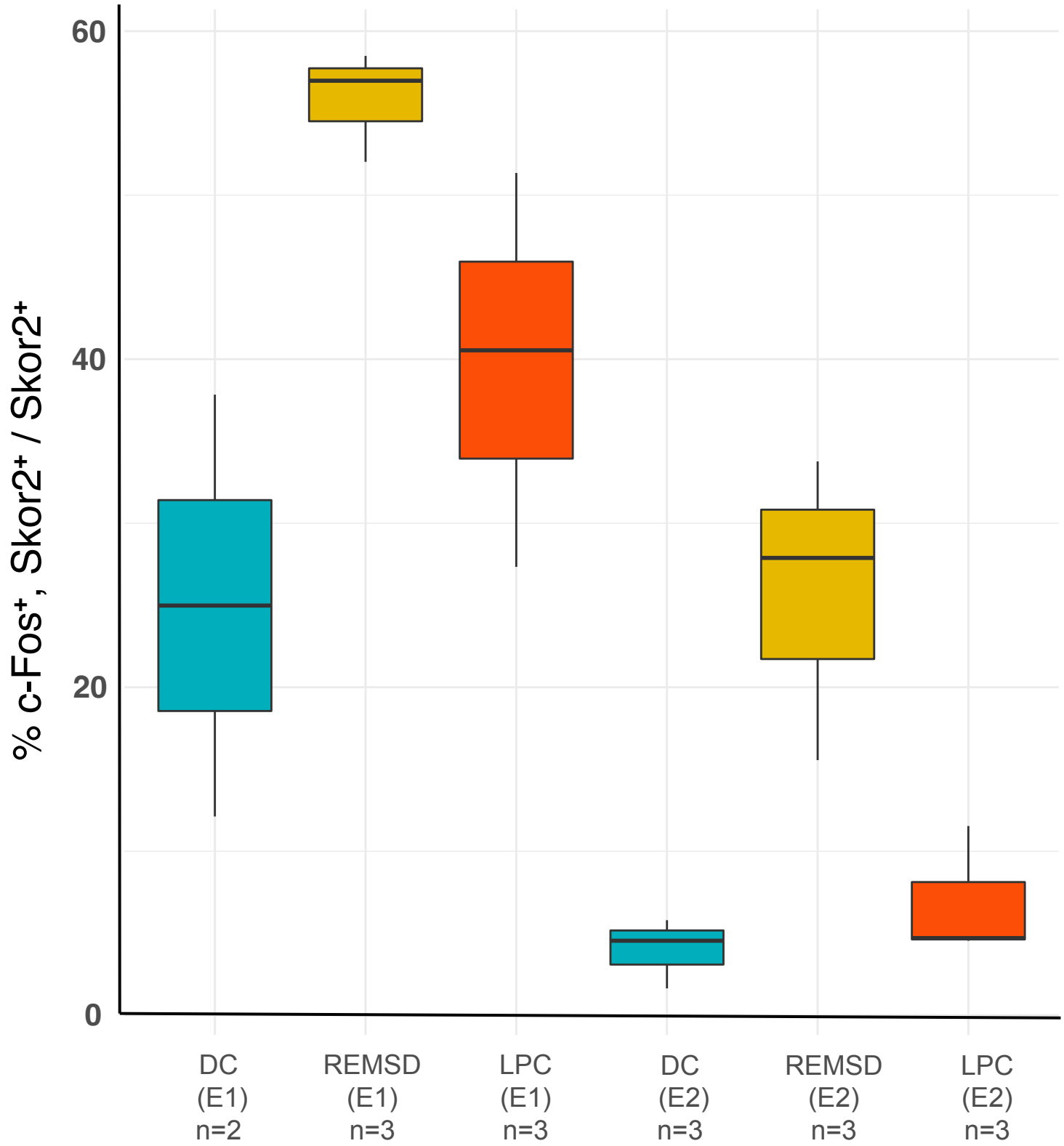

Fig. S7. c-Fos staining efficiency in REM sleep deprivation experiments, before normalisation. Data is presented as percent of c-Fos-positive cells from the dMRF/vlPAG *Skor2*$^{+}$ cells. Experiment groups (DC, REMSD, LPC) and experiment number (E1, E2) is indicated. Due to staining efficiency or other technical variation, the proportion of c-Fos labelled cells differs between the individual experiments (E1 and E2). The difference is systematic, as the experiment groups (DC, REMSD, LPC) show the same trend in labelled cell proportion. The number of animals (n) in each experiment and treatment group is indicated.

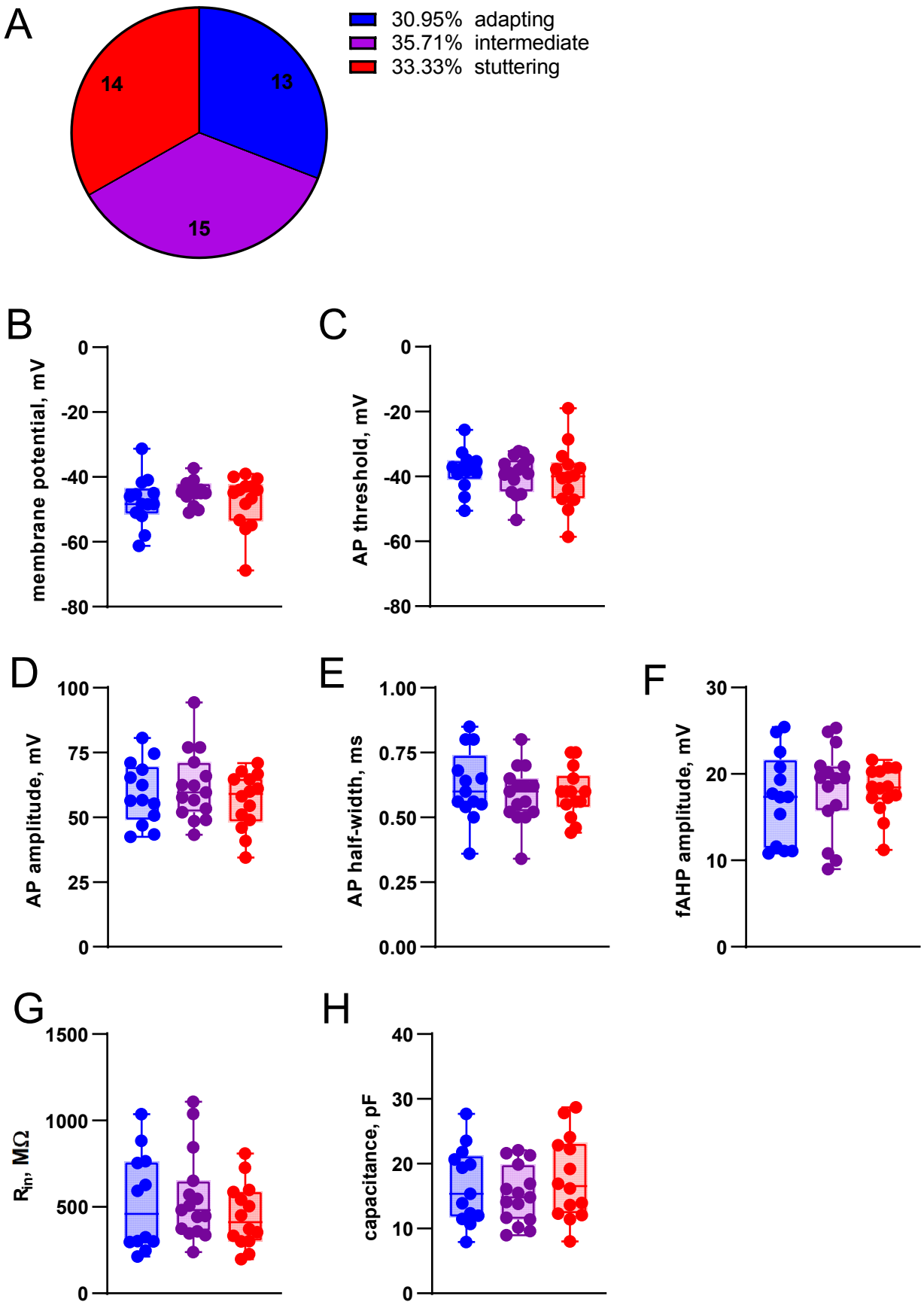

Fig. S8. Classification of the *Skor2*$^{+}$ neurons by the firing patterns. A, The proportion of cells by the assigned firing pattern class. B-H, Comparison of the excitability parameters measured in adapting, intermediate and stuttering GFP^{+} neurons in the *Skor2*$^{GFP/+}$ mouse midbrain by electrophysiology. Boxplots show median, 25 and 75 percentiles with whiskers showing minimum and maximum values. RMP, resting membrane potential; AP, action potential; mAHP and fAHP, medium and fast after-hyperpolarizing potential; R_{in}, input resistance.

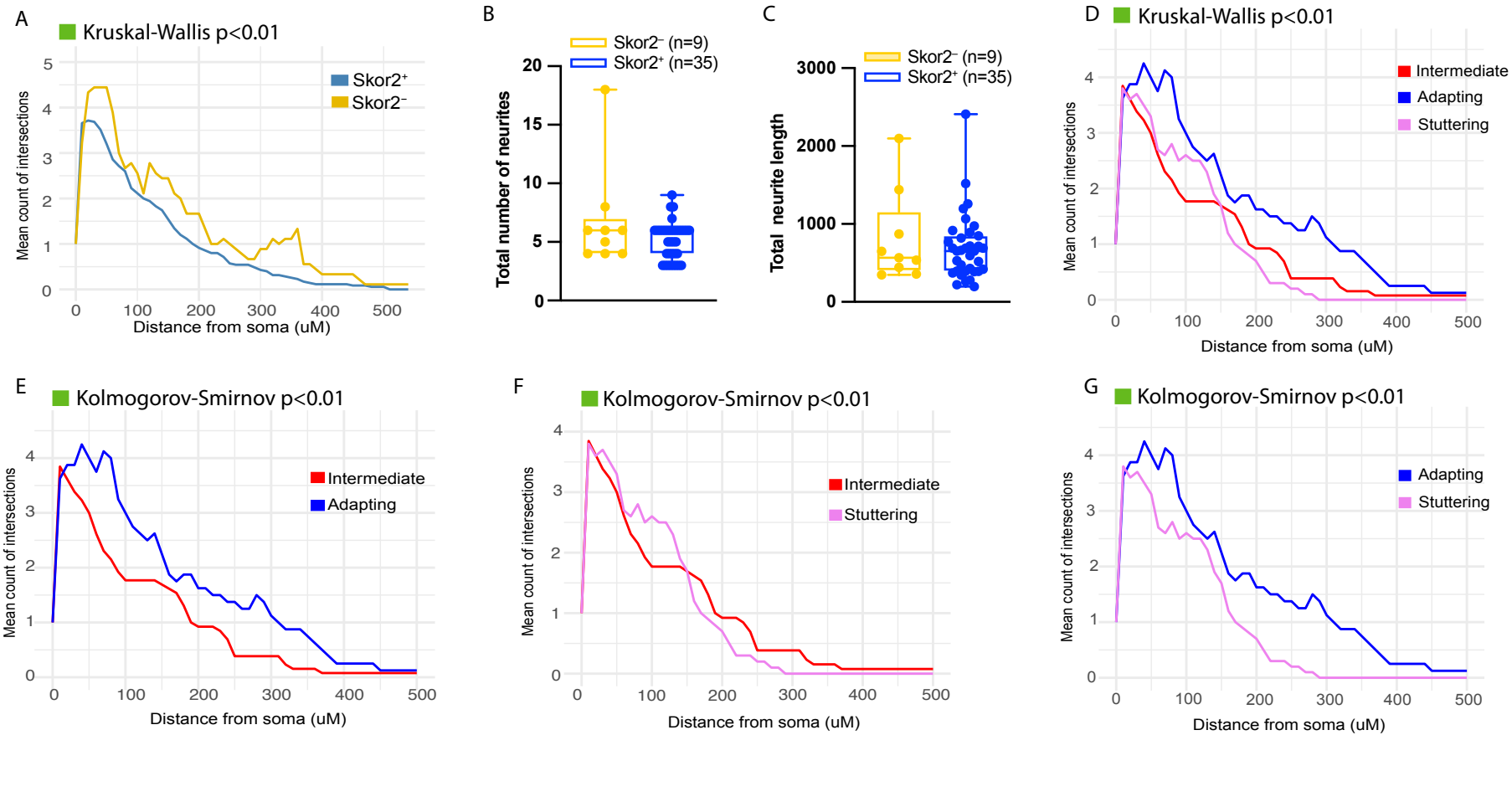

Fig. S9. Comparison of morphological measurements of the *Skor2*+ and *Skor2*- neurons and the *Skor2*+ neuron subclasses

A, Average number of the intersections (+/- SEM) in Sholl analysis of GFP^{+} (*Skor2*$^{+}$, n= 35) and GFP^{-} (*Skor2*$^{-}$, n= 9) cells in the *Skor2*$^{GFP/+}$ mouse midbrain. The distance intervals where significant change (Kruskal-Walls test $p<0.01$) in the number of intersections was observed is highlighted in green. Calculations were conducted with moving window of 50 μm.

B-C, Comparison of the neurite number (B) and length in pixels (C) between the GFP^{+} (*Skor2*$^{+}$, n= 35) and GFP^{-} (*Skor2*$^{-}$, n= 9) cells.

D-G, Average number of the intersections (+/- SEM) in Sholl analysis of GFP^{+} neuron subclasses. The comparative analysis of all three cell classes (D), as well as the pairwise comparisons are shown. The distance intervals where significant change in the number of intersections was observed is highlighted in green. Kruskal-Wallis test of multiple comparisons was used in the comparison of three groups, Kolmogorov-Smirnov test for the pairwise comparison. Significance threshold in both tests was $p<0.01$. Calculations were conducted with moving window of 50 μm.

Table S1. Downregulated genes in the E12.5 *Gata2*^{cko} midbrain.

Click here to download Table S1

Table S2. Complete list of down- and upregulated genes in E12.5 *Gata2*^{cko} dorsal and ventral midbrain, identified in the microarray data analyses.

Click here to download Table S2

Table S3. The gene ontology (GO) terms enriched among the genes downregulated in the *Gata2*^{cko} midbrain. DAVID (https://david.ncifcrf.gov/) was used for the enrichment analysis.

Click here to download Table S3

Table S4. The group identity, experiment ID, number of *Skor2*$^{+}$ cells, number of c-Fos^{+} cells, the percent of c-Fos labelled *Skor2*$^{+}$ cells and the transformed z-scores for each animal in the REM sleep deprivation assay.

Click here to download Table S4

Table S5. Antibodies and mRNA ISH probes used in the study.

Primary antibodies				
Target protein	**Supplier**	**Catalog number**	**Produced in (species)**	**Working concentration**
TH	Millipore	MAB318	mouse	1:500
Ctb	List biological Lab.Inc.	703	goat	1:1000
GFP	Abcam	ab13970	chicken	1:1000
GFP	Abcam	ab290	rabbit	1:500
Neurofilament	DSHB	2H3	mouse	1:500
FoxP1	Abcam	ab16645	rabbit	1:400
Nkx2-2	DSHB	74.5A5	mouse	1:200
Orexin r1 (HCRTR1)	Alomone labs	AOR-001	rabbit	1:100
Orexin r2 (HCRTR2)	Alomone labs	AOR-002	rabbit	1:100
Skor2	Atlas antibodies	HPA046206	rabbit	1:400
Pou4f1(Brn3a)	Santa Cruz Biotechnology	sc-8429	mouse	1:200
RFP	Rockland	600-401-379	rabbit	1:500
c-Fos (FosB)	Abcam	ab11959	mouse	1:500
Secondary antibodies				
rabbit IgG 488	Thermo fisher scientific	A21206	donkey	1:400
rabbit IgG 568	Thermo fisher scientific	A21202	donkey	1:400
goat IgG 568	Thermo fisher scientific	A11057	donkey	1:400
mouse IgG 568	Thermo fisher scientific	A32744	donkey	1:400
mouse IgG 647	Thermo fisher scientific	A31571	donkey	1:400
rabbit IgG 647	Thermo fisher scientific	A31573	donkey	1:400
chicken IgG 488	Thermo fisher scientific	A32931	goat	1:400

mRNA probes		
Target gene	**Source**	**Clone number (if applicable)**
Gad1	RZPD	IRAVp968CM67D6
Gata2	Lilleväli et al., 2004	n/a

Gata3	Lilleväli et al., 2004	n/a
Lhx5	Source Bioscience	IMAGE ID 6830059
Nkx2-2	RZPD	IMAGE clone 480100
Six3	Source Bioscience	IMAGp998B1912702Q
mouse Skor2	Source Bioscience	IMAGE ID 6853809
Slc17a6 (Vglut2)	Guimera et al., 2006	n/a
Sox14	Source Bioscience	IMAGp998A2414391Q
Tal1	Source Bioscience	IRAVp968D09118D
Tal2	RZPD	IRCLp5011D0623D
Zfpm1	Source Bioscience	IMAGE ID 3585094
Zfpm2	Source Bioscience	IRAVp968B06115D
rat Skor2	see Materials and Methods	n/a